



21 **Abstract.** The range of boundary layer stability profiles, from the surface to 500 m above ground level,
22 present in radiosonde observations from two continental interior (South Pole and Dome Concordia) and
23 three coastal (McMurdo, Georg von Neumayer III, and Syowa) Antarctic sites, is examined using the self-
24 organizing maps (SOMs) neural network algorithm. A wide range of potential temperature profiles is
25 revealed, from shallow boundary layers with strong near-surface stability to deeper boundary layers with
26 weaker or near-neutral stability, as well as profiles with weaker near-surface stability and enhanced
27 stability aloft, above the boundary layer. Boundary layer regimes were defined based on the range of
28 profiles revealed by the SOM analysis. Twenty boundary layer regimes were identified to account for
29 differences in stability near the surface as well as above the boundary layer. Strong, very strong, or
30 extremely strong stability, with vertical potential temperature gradients of 5 to in excess of 30 K (100 m)
31 ⁻¹, occurred more than 80% of the time at South Pole and Dome Concordia in the winter. Weaker stability
32 was found in the winter at the coastal sites, with moderate and strong stability (vertical potential
33 temperature gradients of 1.75 to 15 K (100 m)⁻¹) occurring 70% to 85% of the time. Even in the summer,
34 moderate and strong stability is found across all five sites, either immediately near the surface or aloft,
35 just above the boundary layer. While the mean boundary layer height at the continental interior sites was
36 found to be approximately 50 m, the mean boundary layer height at the coastal sites was deeper, around
37 110 m. Further, a commonly described two stability regime system in the Arctic associated with clear or
38 cloudy conditions was applied to the 20 boundary layer regimes identified in this study to understand if
39 the two-regime behavior is also observed in the Antarctic. It was found that moderate and strong stability
40 occur more often with clear than cloudy sky conditions, but weaker stability regimes occur almost equally
41 for clear and cloudy conditions.



42 1 Introduction

43 Strong temperature inversions in Antarctica are the result of predominantly high albedo ice-
44 covered surfaces and low sun angle in the summer and polar night in winter. All these factors contribute
45 to prolonged surface radiative cooling which often results in statically stable boundary layers (King and
46 Turner, 1997; Andreas et al., 2000) with temperature inversions sometimes exceeding 20 K (Lettau and
47 Schwerdtfeger, 1967; Phillpot and Zillman, 1970). Increased solar radiation and warmer surface
48 temperatures can result in near neutral or weakly stable conditions during the summer. Similar stability
49 conditions can also occur at other times of year as a result of increased wind speeds or increased
50 downwelling longwave radiation due to cloud cover (Hudson and Brandt, 2005; Stone and Kahl, 1991).
51 This study aims to investigate the range of boundary layer stability that exists throughout the year at two
52 continental interior sites and three coastal sites in Antarctica (Figure 1).

53 A previous study for McMurdo Station analyzed the range of boundary layer stability regimes
54 present during the year-long Department of Energy (DOE) Atmospheric Radiation Measurement (ARM)
55 West Antarctic Radiation Experiment (AWARE) campaign (Dice and Cassano, 2022). A strong
56 seasonality of varying boundary layer stability was found, with the winter conditions dominated by
57 strongly stable boundary layers (61% of the time), and summer conditions dominated by weak stability
58 (83% of the time). Increased wind speeds in the winter were found to be responsible for reducing strong
59 near-surface stability. This reduction of stability occurred near the surface while enhanced stability
60 remained aloft in some cases. The results presented below aim to expand the analysis of boundary layer
61 stability in Dice and Cassano (2022) to both continental and coastal locations across Antarctica.

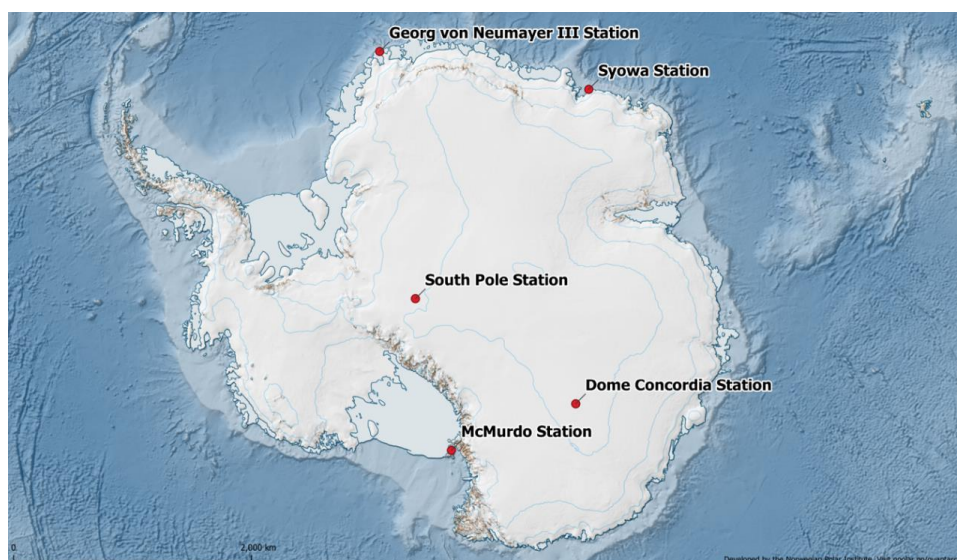
62 Data from two additional coastal stations, Georg von Neumayer Station III (Neumayer Station)
63 and Syowa Station (Figure 1) will also be analyzed, in addition to revisiting the data at McMurdo Station
64 described above. Previously published results found surface-based temperature inversions occurred year-
65 round at Neumayer Station, with a maximum frequency in the winter and a minimum in the summer, with
66 75% of the inversions having a strength of more than 1 K, and some up to 25 K, especially in the winter
67 (König-Langlo and Loose, 2007; Silva et al., 2022). Some of the temperature profile structures observed
68 by Silva et al. (2022) revealed multiple inversions within the same profile. This is similar to McMurdo
69 Station where enhanced stability was often found to exist above a layer of weaker stability (Dice and
70 Cassano, 2022). Cassano et al. (2016) found that stable boundary layer conditions occur 83% of the year
71 over the northwestern Ross Ice Shelf (approximately 100 km from McMurdo Station), while neutral
72 conditions occur 17% of the time. Further, 50% of the summer season was characterized by weakly
73 unstable conditions, while stable stratification is dominant in the other three seasons (84% to 94%).

74 The continental interior of Antarctica is characterized by a short summer and a long, coreless
75 winter (Hudson and Brandt, 2005). Stronger inversions and colder temperatures are often characteristic of
76 higher elevation, continental interior sites (Phillpot and Zillman, 1970; Comiso, 1994; Zhang, et al.,
77 2011), compared to coastal locations with weaker inversions and warmer temperatures (Phillpot and
78 Zillman, 1970; Cassano et al., 2016). Continental interior sites also have greater inversion frequency than
79 coastal sites, with inversion frequency in the fall and winter close to 100% (Zhang et al., 2011). At South
80 Pole Station, inversions were found to be more common and stronger in the winter than in the summer.
81 Hudson and Brandt (2005) also found inversions in the summer at Dome C to be stronger than those at
82 South Pole. Inversions near the surface at Dome C can reach to 1 K m⁻¹ during polar night, and even
83 stronger inversions, at 10 to 15 m above the surface, of up to 2.5 K m⁻¹ have been observed (Genthon et
84 al., 2013).



85 Boundary layer stability in the polar regions in the winter has often been described as existing in
86 two distinct states (weak or strongly stable) driven by changes in cloud cover. The weakly stable regimes
87 occur under cloudy conditions, with increased downwelling longwave radiation warming the surface and
88 reducing stability. In contrast, clear sky conditions allow for strong radiative cooling and strong stability
89 (Stone and Kahl, 1991; Mahrt et al., 1998; Mahrt, 2014; Solomon et al., 2023). Stone and Kahl (1991)
90 described boundary layer stability at the South Pole as being in either a weakly stable or strongly stable
91 regime, associated with cloudy or clear conditions, respectively throughout the summer of 1986. Solomon
92 et al. (2023) distinguished between wintertime clear and cloudy regimes in the Arctic, during the
93 Multidisciplinary drifting Observatory for the Study of Arctic Climate (MOSAIC) campaign, to evaluate
94 model predictions of near-surface meteorological conditions including boundary layer stability. They
95 separated clear and cloudy regimes using the minima between the two peaks in the observed bimodal
96 probability distribution function (PDF) of net longwave radiation. Following Solomon et al. (2023) we
97 will identify clear and cloudy regimes based on the PDFs of net longwave radiation to determine if this
98 bimodal view of clouds, and associated boundary layer stability, found in the Arctic is also applicable to
99 coastal and interior sites across the Antarctic continent. We will also study how the clear-cloudy regimes
100 relate to the continuous range of stability regimes identified in this study.

101 This paper begins with a description of the observations from five Antarctic sites and details of
102 the methods used to analyze the data at these sites (Section 2). The results of this analysis will describe
103 the range and frequency of boundary layer stability profiles (up to 500 m AGL) at the sites (Section 3).
104 Additionally, differences in boundary layer stability associated with clear and cloudy conditions will be
105 presented. The results section will be followed by a discussion and comparison across coastal versus
106 continental interior locations (Section 4). A summary of these findings will follow, and the next steps in
107 this research will be identified (Section 5).



108 *Figure 1: Location of study sites (red dots with station names) across the Antarctic continent. Map*
109 *courtesy of Quantarctica (Matsuoka et al., 2018).*



110 **2 Data and Methods**

111 **2.1 Data**

112 The analysis presented in this paper is based on radiosonde and surface longwave radiation
113 observations from three coastal (McMurdo Station, Neumayer Station, and Syowa Station) and two
114 continental interior sites (South Pole Station, Dome Concordia Station) (Figure 1, Table 1, hereafter these
115 five stations are referred to as McMurdo, Neumayer, Syowa, South Pole, and Dome C). The period of
116 data used in the analysis at these five sites range from 13 months (McMurdo) to 19 years (Syowa). The
117 differing time period evaluated at each site is due to varying amounts of time when radiosonde and
118 radiation data are both continuously available, as well as periods of time when data was readily
119 accessible. At McMurdo, this time period was chosen to coincide with availability of both radiosonde and
120 radiation data from the AWARE campaign, which was previously analyzed by Dice and Cassano (2022).
121 The Neumayer dataset is shorter than those at Syowa, Dome C, and South Pole, as Neumayer was not
122 fully operational until 2009, and from 2009 to 2018, only 5 s temporal resolution radiosonde data was
123 available. This data did not have sufficient vertical resolution for this study, thus only data after 2018 with
124 1 s temporal resolution was used. Syowa, Dome C, and South Pole all have longer continuous radiosonde
125 and radiation datasets, that are easily accessible, lasting more than approximately 15 years.

126 South Pole is a high-elevation (2,835 m) continental interior site where strong surface inversions
127 and extremely cold temperatures dominate (Zhang et al., 2011), and strong stability is almost constantly
128 observed, especially in the winter (Phillpot and Zillman, 1970). The radiosonde data from the South Pole
129 were retrieved from the Antarctic Meteorological Research and Data Center from 1 January 2005 to 29
130 September 2021. Radiosonde launches occur once daily at 2100 UTC for most of the year, with twice
131 daily launches at approximately 0900 UTC and 2100 UTC during the short austral summer.

132 Dome C is another high-elevation (3,233 m) continental interior site characterized by cold
133 temperatures and strong surface inversions, which occur throughout most of the year, and in the winter on
134 a nearly permanent basis (Genthon et al., 2013; Pietroni et al., 2014, Vignon et al., 2017). The radiosonde
135 data from Dome C are provided by the Antarctic Meteo-Climatological Observatory from 21 January
136 2006 to 14 October 2021. The radiosonde launches at Dome C are performed once daily at 1200 UTC
137 year-round.

138 McMurdo is a coastal site located at the edge of the Ross Ice Shelf on the southwestern tip of
139 Ross Island. The proximity of the Ross Ice Shelf, sea ice, open water, and the complex local topography
140 near McMurdo results in a wide range of boundary layer stability types compared to the continental
141 interior sites (Dice and Cassano, 2022). The McMurdo radiosonde data are from the DOE AWARE
142 campaign (Lubin et al., 2017, 2020; Silber et al., 2018), which occurred at McMurdo from 20 November
143 2015 to 3 January 2017. The radiosonde launches during AWARE occurred twice per day at 1000 UTC
144 and 2200 UTC.

145 Neumayer is near sea-level and located on the Ekström Ice Shelf, a relatively flat and
146 homogeneous site. The meteorology and near-surface conditions are frequently influenced by large-scale
147 cyclonic activity and sea ice fluctuations (Silva et al., 2022) resulting in changing boundary layer
148 conditions. The radiosonde data from Neumayer are from the Baseline Surface Radiation Network
149 (BSRN) from 1 June 2018 to 31 January 2021. Radiosonde launches occur once daily at approximately
150 1200 UTC, and twice daily during the summer months when conditions allow, at 0500 UTC and 1200
151 UTC.



152 Syowa is located on East Ongul Island in Lutzow-Holm Bay near sea level, with some low-
 153 elevation slopes around it, and like the other coastal sites, it experiences warmer surface temperatures
 154 compared to the continental interior. Syowa also experiences occasional strong wind due to katabatic flow
 155 from the continental interior (Murakoshi, 1958). The radiosonde data from Syowa are from the Office of
 156 Antarctic Observation Japan Meteorological Agency (pers. comm. Yutaka Ogawa) from 1 February 2001
 157 to 23 January 2020. Radiosonde launches occur twice daily at 1130 and 2330 UTC.

158 Longwave radiation data were also obtained for all five sites to identify the clear and cloudy sky
 159 conditions following the methods from Solomon et al. (2023). The radiation data are from the BSRN,
 160 except at McMurdo where the data is from the AWARE campaign.

161 *Table 1: Information for each of the five study sites: South Pole, Dome C, McMurdo, Neumayer, and*
 162 *Syowa. From left to right, the columns indicate: study site, coordinates and elevation above sea level*
 163 *(ASL) of each site, site location type, the type of radiosonde and accuracy of the temperature and wind*
 164 *measurements, respectively, the time period of the radiosonde launches, and the number of radiosonde*
 165 *launches in the dataset.*

Station	Coordinates, Elevation	Site Type	Instrument Type and Accuracy	Time Period of Radiosonde Launches	Number of Radiosonde Launch Profiles
South Pole	-89.98°S, 24.80°W; 2,836 m ASL	Interior plateau	Vaisala RS41-SGP radiosondes; 0.2 K, 0.5 m s ⁻¹	01 Jan 2005-29 Sep 2021	8,587
Dome Concordia	-75.10°S, 123.33°E; 3,251 m ASL	Interior plateau	RS-92 radiosondes; 0.2 K, 0.2 m s ⁻¹	21 Jan 2006- 14 Oct 2021	5,147
McMurdo	-77.85°S, 166.66° E; 10.1 m ASL	Coastal; Ross Island	RS-92 radiosondes; 0.2 K, 0.2 m s ⁻¹	30 Nov 2015- 03 Jan 2017	786
Georg von Neumayer	-70.65°S, -8.17°W; 38 m ASL	Coastal; Ekström Ice Shelf	Vaisala, RS41-SGP radiosondes; 0.2 K, 0.5 m s ⁻¹	01 Jun 2018- 31 Jan 2021	1,220
Syowa	-69.00°S, 39.58°W; 18.4 m ASL	Coastal; East Ongul Island	Meisei RS-11G radiosondes; 0.5 K, 2 m s ⁻¹	01 Feb 2007- 23 Jan 2020	6,390



166 **2.2 Methods**

167 **2.2.1 Self-Organizing Map**

168 The goal of this paper is to analyze and compare the variability in boundary layer stability,
169 defined by potential temperature profiles, at five Antarctic research stations (Figure 1). Hundreds of
170 thousands of radiosonde profiles (Table 1), for each of the five sites, will be analyzed. The self-organizing
171 map, or SOM, algorithm is used to objectively identify patterns in the potential temperature profiles that
172 represent the range of conditions in the radiosonde observations.

173 The SOM algorithm is an unsupervised artificial neural network that groups similar patterns in
174 the training data into a user-specified number of patterns, which span the range of conditions in the
175 training data. The iterative training proceeds until the squared difference between the training data and the
176 SOM patterns is minimized (Kohonen et al., 1996; Hewitson and Crane, 2002; Cassano et al., 2015). The
177 resulting two-dimensional array of patterns is the master SOM, or simply the SOM. The SOM is
178 organized such that similar patterns are located adjacent to each other, while the most distinct patterns are
179 on opposite sides (Cassano et al., 2016). The SOMs presented here are trained using potential temperature
180 gradient profiles from the radiosonde observations. The potential temperature gradient profiles ($d\theta/dz$)
181 were used to train the SOM because this gradient defines the local static stability in the profile and allows
182 for classification of boundary layer stability regimes across seasons and sites. The SOMs in this study
183 were trained using the SOM-PAK software (<http://www.cis.hut.fi/research/som-research>), the details of
184 which are described by Kohonen et al. (1996).

185 The radiosonde data is interpolated onto a regular vertical grid before applying the SOM
186 algorithm, as described in Dice and Cassano (2022). Radiosonde profiles from all sites were interpolated
187 to a 5 m grid from 20 to 500 m above ground level. The lowest height of 20 m was selected since near-
188 surface warm biased temperatures are often present in radiosonde data observed below this height in
189 many profiles at the five study sites (Schwartz and Doswell, 1991; Mahesh et al., 1997). The top height of
190 500 m was chosen since this height encompasses the boundary layer features of interest.

191 To decide on the number of patterns to be identified by the SOM algorithm, several tests were
192 performed to find the appropriate SOM size to adequately represent the range of boundary layer profiles
193 present at each of the five sites. Unlike other iterative, unsupervised training algorithms, the SOM does
194 not identify distinct patterns, but a range of patterns which vary smoothly across the boundary layer states
195 observed in the radiosonde data. Identifying the proper SOM size is important for visualizing the full
196 range of boundary layer stability profiles present in the training data (Reusch et al., 2005; Cassano et al.,
197 2015). Too small of a SOM will result in important differences in the training data being lost in the few
198 generalized patterns, and too large of a SOM will be difficult to visualize, and only a few samples from
199 the training data may correspond, or “map” to each SOM pattern. Several SOM sizes were tested for this
200 analysis: 3 x 2 (6 patterns), 4 x 3 (12 patterns), 5 x 4 (20 patterns), 6 x 5 (30 patterns), and 7 x 6 (42
201 patterns). This initial evaluation of different SOM sizes found that a 6x5 SOM (Figures 2, 4, 6, 8, and 10)
202 best represented the boundary layer states present across the training data at all five sites. The 30 patterns
203 in the 6x5 SOM span the range of potential temperature profile types present in the training data, which
204 represents the hundreds to thousands of profiles (Table 1) from each of the five sites.

205 Once the SOM is trained, each individual radiosonde profile from the training data is “mapped”
206 to a single pattern in the SOM that it is most similar to by finding the pattern that has the smallest squared
207 difference between the radiosonde profile and the SOM-identified pattern. This mapping procedure
208 produces a list of best matching units, or BMUs, which identify the potential temperature gradient profiles
209 in the training data that correspond to each pattern in the SOM. Using this list, mean potential temperature



210 gradient and mean potential temperature anomaly (defined relative to the potential temperature at 500 m)
211 profiles are calculated and used to visualize the range of stability profiles present at each site (Figures 2,
212 4, 6, 8 and 10). The list of BMUs is also used to calculate the frequency of occurrence of each SOM
213 pattern and can be used to identify how boundary layer stability varies annually and seasonally. The
214 seasons are defined in this study as follows: summer (DJ), fall (FMA), winter (MJJA), and spring (SON).
215 These seasons are identified as such following previous definitions of Antarctic seasons (Cassano et al.,
216 2016, Nigro et al., 2017).

217 **2.2.2 Boundary Layer Regime Definitions**

218 The SOM analysis described above provides a relatively compact way to visualize the range of
219 boundary layer conditions present in the radiosonde observations, as well as their seasonality at the
220 various sites. However, this analysis does not allow for direct, quantitative comparison across the five
221 sites since unique SOMs are defined for each location. Thus, to compare the range of boundary layer
222 stability present at each of the five sites (Figure 1) the potential temperature gradient profiles are used to
223 define boundary layer stability regimes. The stability regime definitions are based on both the near-
224 surface stability (20 m to 50 m) and stability above the height of the boundary layer (up to 500 m) and
225 boundary layer depth.

226 Six near-surface stability regimes were defined (Table 2, left column) based on the potential
227 temperature gradient between 20 m and 50 m above ground, as this depth captures the near-surface
228 conditions while avoiding measurement errors below 20 m. The near-surface stability regimes range from
229 near neutral (NN; $d\theta/dz < 0.5 \text{ K (100 m)}^{-1}$) to extremely strongly stable (ESS; $d\theta/dz > 30 \text{ K (100 m)}^{-1}$).
230 Various thresholds to distinguish near neutral (NN), weak (WS), moderate (MS), strong (SS), very strong
231 (VSS), and extremely strong (ESS) stability were evaluated, and the thresholds listed in Table 2 were
232 found to best separate meaningful differences in near-surface stability across all five sites. These
233 thresholds were also evaluated, and found to be appropriate, in a separate study based on profiles
234 observed over Arctic sea ice as part of the MOSAiC expedition (Jozef et al. 2023).

235 It was also noted that many of the SOM patterns were characterized by a layer of stronger
236 stability above weaker stability near the surface, which was also noted by Dice and Cassano (2022) at
237 McMurdo. Therefore, the stability above the boundary layer is also used to define the overall stability
238 regime (Table 2). This requires identifying the top of the boundary layer, which is done following Jozef et
239 al. (2022) by using profiles of the bulk Richardson number. The bulk Richardson number is defined as the
240 ratio of buoyant turbulence production, or suppression, to mechanical generation of turbulence by wind
241 shear. A critical bulk Richardson number indicates the point at which turbulence cannot be sustained
242 (Stull, 1988). The boundary layer height is defined as the point in the profile where the bulk Richardson
243 number exceeds a critical value of 0.5 and remains above that critical value for at least 20 meters
244 consecutively.

245 Aloft stability regimes were determined with the same potential temperature gradient thresholds
246 as were used for the near surface stability regimes (Table 2). The maximum potential temperature
247 gradient above the boundary layer height and below 500 m was used to identify the aloft stability regimes.
248 Aloft-stability regimes were applied to any potential temperature gradient profile with a greater stability
249 aloft compared to the near-surface stability of that profile. No aloft stability regime is applied for cases
250 with the strongest stability near the surface.

251 Boundary layer stability regimes were also defined based on the depth of the boundary layer. In
252 analyzing all the boundary layer profiles it was found that there was a clear distinction between a group of
253 NN and WS regimes with boundary layer heights less than 125 m, and NN and WS regimes with



254 boundary layer heights much greater than 125 m. Thus, a very shallow mixed (VSM) stability regime was
 255 defined to distinguish these cases, specifically for the NN and WS regimes with boundary layer depths
 256 less than 125 m.

257 The near-surface and aloft stability regimes, along with the VSM regimes, were combined into an
 258 overall stability regime, as listed in Table 3. For example, a profile identified as having near-neutral
 259 stability near the surface with strong stability above the boundary layer, would be identified as near-
 260 neutral, strong stability aloft, or NN-SSA. Thus, we end up with “stability groupings” with the same near
 261 surface stability for multiple regimes, but with varying stability aloft. One example of these groupings is
 262 the following: NN (near-neutral), NN-WSA (near-neutral, weak stability aloft), NN-MSA (near-neutral,
 263 moderate stability aloft), and NN-SSA (near-neutral, strong stability aloft; Table 3).

264 *Table 2: Boundary Layer Regime definition scheme. The left column of the table shows the potential*
 265 *temperature gradient ($d\theta/dz$ in $K (100 m)^{-1}$) thresholds used to define each of the six basic near-surface*
 266 *stability regimes from 20 m to 50 m. The middle column shows how the very shallow mixed layer*
 267 *definition was applied to NN and WS cases. The third column shows the maximum potential temperature*
 268 *gradient thresholds ($d\theta/dz$ in $K (100 m)^{-1}$) for the aloft stability regimes.*

Near-Surface Stability	Very Shallow Mixed Layer	Stability Above Boundary Layer (“Aloft”)
Near-Neutral (NN): $d\theta dz^{-1} < 0.5 K (100 m)^{-1}$	If near-surface stability = NN or WS and ABL height <125 m ➤ Near-surface stability = Very-Shallow Mixed (VSM)	
Weak Stability (WS): $d\theta dz^{-1} \geq 0.5 K (100 m)^{-1}$ and $< 1.75 K (100 m)^{-1}$		Weak Stability Aloft (-WSA): $d\theta dz^{-1} \geq 0.5 K (100 m)^{-1}$ and $< 1.75 K (100 m)^{-1}$
Moderate Stability (MS): $d\theta dz^{-1} \geq 1.75 K (100 m)^{-1}$ and $< 5 K (100 m)^{-1}$		Moderate Stability Aloft (-MSA): $d\theta dz^{-1} \geq 1.75 K (100 m)^{-1}$ and $< 5 K (100 m)^{-1}$
Strong Stability (SS): $d\theta dz^{-1} \geq 5 K (100 m)^{-1}$ and $< 15 K (100 m)^{-1}$		Strong Stability Aloft (-SSA): $d\theta dz^{-1} \geq 5 K (100 m)^{-1}$
Very Strong Stability (VSS): $d\theta dz^{-1} \geq 15 K (100 m)^{-1}$ and $< 30 K (100 m)^{-1}$		Very Strong Stability Aloft (-VSSA): $d\theta dz^{-1} \geq 15 K (100 m)^{-1}$
Extremely Strong Stability (ESS): $d\theta dz^{-1} \geq 30 K (100 m)^{-1}$		Extremely Strong Stability Aloft (-ESSA): $d\theta dz^{-1} \geq 30 K (100 m)^{-1}$

269 Regimes where no increased stability aloft is present (NN, WS, MS, SS, VSS, or ESS) as well as
 270 the VSM-WSA will be referred to as “basic near-surface stability regimes”. The reasoning for including
 271 VSM-WSA in the basic near-surface stability regimes is that this regime is defined both by stability as
 272 well as boundary layer depth. The VSM regime is derived from the same conditions that define the NN
 273 and WS regimes, but in the VSM regime, a much shallower boundary layer exists (less than 125 m). The -



274 WSA in this regime is consistent with the potential temperature gradient that defines the VSM regime as a
 275 whole and is thus considered as part of the basic near-surface stability regimes. Each stability grouping is
 276 identified by a distinct color (Table 3): NN – brown; VSM – red; WS – green; MS – blue; SS – purple;
 277 VSS – pink; ESS – indigo), in which the darkest color is the basic near-surface regime (no increased
 278 stability aloft), and with decreasing color intensity as stability aloft in that regime grouping increases.

279 *Table 3: Boundary Layer Regime acronyms and color codes. On the left is the color and acronym used to*
 280 *represent each of the 20 stability regimes in figures and tables throughout this paper, and the full regime*
 281 *name is spelled out on the right. The basic near-surface stability regimes are denoted in bold font.*

Regime Color and Acronym	Regime Full Name
NN	Near Neutral
NN-WSA	Near Neutral- Weak Stability Aloft
NN-MSA	Near Neutral- Moderate Stability Aloft
NN-SSA	Near Neutral- Strong Stability Aloft
VSM-WSA	Very Shallow Mixed- Weak Stability Aloft
VSM-MSA	Very Shallow Mixed- Moderate Stability Aloft
VSM-SSA	Very Shallow Mixed- Strong Stability Aloft
WS	Weak Stability
WS-MSA	Weak Stability- Moderate Stability Aloft
WS-SSA	Weak Stability- Strong Stability Aloft
MS	Moderate Stability
MS-SSA	Moderate Stability- Strong Stability Aloft
MS-VSSA	Moderate Stability- Very Strong Stability Aloft
MS-ESSA	Moderate Stability- Extremely Strong Stability Aloft
SS	Strong Stability
SS-VSSA	Strong Stability- Very Strong Stability Aloft
SS-ESSA	Strong Stability- Extremely Strong Stability Aloft
VSS	Very Strong Stability
VSS-ESSA	Very Strong Stability- Extremely Strong Stability Aloft
ESS	Extremely Strong Stability



282 2.2.3 Clear and Cloudy Regime Classification

283 As mentioned in the Introduction, wintertime boundary layer stability in the polar regions is often
284 described to be made up of two regimes, which differ based on the presence or absence of clouds and the
285 associated differences in downwelling longwave radiation. This two-regime system is often defined as a
286 “clear regime” with low values of downwelling longwave radiation, strong surface radiative cooling, and
287 strong stability, and a “cloudy regime”, with enhanced downwelling longwave radiation, surface warming
288 and decreased near-surface stability (Phillpot & Zillman, 1970; Stone and Kahl, 1991; Solomon et al.,
289 2023). Here, we will assess how the frequency of the 20 boundary layer regimes (Table 2) relate to the
290 more commonly defined clear (strongly stable) and cloudy (weakly stable) regimes to evaluate the use of
291 this more nuanced view of the relationship between boundary layer stability and cloud cover.

292 To determine the conditions with which the boundary layer regimes defined in Table 2 occur, we
293 follow the approach of Solomon et al. (2023) that used net longwave radiation observations taken over the
294 Arctic sea ice during the MOSAiC expedition to define clear and cloudy conditions. They found that
295 during the winter there was a bimodal distribution of net longwave radiation. The minimum in frequency
296 between the two peaks of this distribution was used to define clear and cloudy states, which were found to
297 have distinct distributions of downwelling longwave radiation (Solomon et al. 2023). Following Solomon
298 et al. (2023) this analysis will be completed only in the winter season.

299 PDFs of wintertime net longwave radiation are calculated at the five study sites (Figures S1 to
300 S5) to determine if bimodal distributions of net longwave radiation are found at coastal and interior
301 Antarctic sites, like what was found in the Arctic. Then, as in Solomon et al. (2023) we determine if
302 distinct distributions in downwelling longwave radiation are present, which serve as a proxy for clear
303 (small values of downwelling longwave radiation) or cloudy (large values of downwelling longwave
304 radiation) conditions. Solomon et al. (2023) used the minima in the net longwave radiation PDF as a
305 threshold to define clear and cloudy regimes. In this study, we define an overlap ratio (defined below) that
306 quantifies how distinct the distributions of downwelling longwave radiation are for a given net longwave
307 radiation threshold used to separate clear and cloudy states. For the identified net longwave radiation
308 threshold, we create two PDFs of downwelling longwave radiation (Figures S1 to S5) based on the subset
309 of observations corresponding to net longwave radiation values above (cloudy) or below (clear) the net
310 longwave radiation threshold. Using the two downwelling longwave radiation PDFs, we determine the
311 total number of clear cases, cloudy cases, and the number of coincident cases where the clear and cloudy
312 PDFs overlap. The overlap ratio is calculated as the number of overlapping cases divided by the total
313 number of clear and the total number of cloudy cases, and the final overlap ratio is the maximum of these
314 two ratios. This overlap ratio quantifies how much overlap exists between the clear and cloudy
315 downwelling longwave radiation PDFs and distinct clear and cloudy PDFs are characterized by low
316 overlap ratios. The overlap ratio is calculated for each value of net longwave radiation (from the
317 minimum to the maximum observed), at 1 W m^{-2} intervals, at each site. The minimum overlap ratio at
318 each site, from the calculations every 1 W m^{-2} , defines the net longwave radiation threshold identifying
319 the most distinct distributions of downwelling longwave radiation for clear and cloudy cases. It generally
320 corresponds to within a few W m^{-2} of the minimum in bimodal PDF of net longwave radiation (vertical
321 black line in Figures S1 to S5). The dates and times corresponding to the clear and cloudy states were
322 used to determine the frequency of boundary layer stability regimes for the two states.



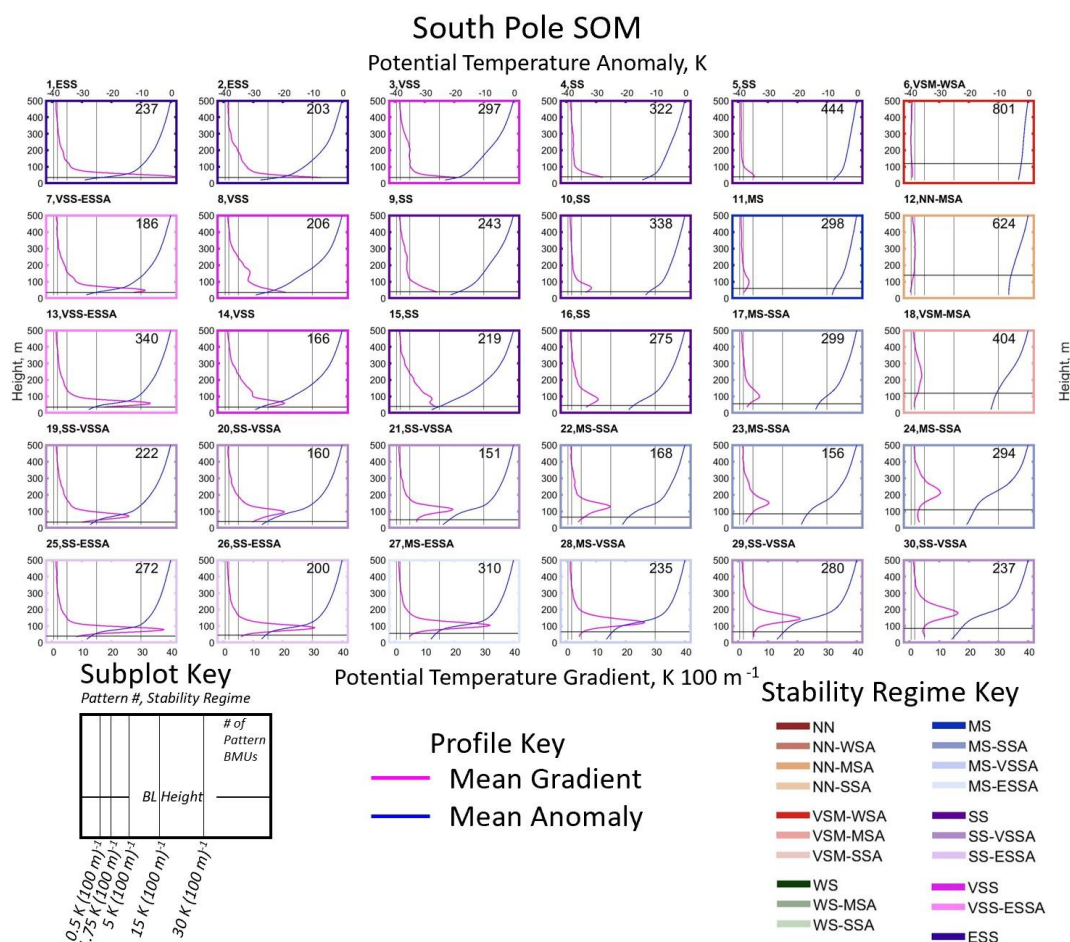
323 **3 Results**

324 **3.1 South Pole**

325 At a high-plateau, continental interior site such as South Pole, it is expected that strong stability
326 will be present throughout much of the year (Phillpot and Zillman, 1970; Comiso, 1994; Hudson and
327 Brandt, 2005; Zhang, et al., 2011). The SOM in Figure 2 shows the range of potential temperature
328 profiles (anomaly and gradient) across 16 years of radiosonde observations at South Pole, as well as the
329 stability regime (colored outline and label in top left of each pattern) corresponding to the mean profiles
330 in each SOM pattern. The left side of the SOM is dominated by the strongest stability patterns, and
331 stability decreases from left to right, with the weakest stability patterns in the upper right corner. Potential
332 temperature gradients more than 5 K (100 m)^{-1} in nearly all of the SOM-identified patterns in Figure 2,
333 with many greater than $15 \text{ K (100 m)}^{-1}$, and some even greater than $30 \text{ K (100 m)}^{-1}$, shows that strong
334 stability is in fact common at this site. Potential temperature gradients in excess of $15 \text{ K (100 m)}^{-1}$,
335 corresponding to our VSS regime (Table 2), are rarely observed outside of the interior of Antarctica, even
336 in the Arctic (Jozef et al., 2023). Potential temperature gradients less than $1.75 \text{ K (100 m)}^{-1}$,
337 corresponding to NN or WS regimes, occur only in patterns 6, 12, and 18 in the upper right of the SOM,
338 emphasizing the dominance of strong stability at South Pole.

339 The height of the maximum potential temperature gradient within the profile varies across the
340 SOM, often being located very close to the surface, as in the top left corner of the SOM, but sometimes
341 the maximum gradient is located above a layer of decreased stability near the surface, as is in the bottom
342 two rows of the SOM. These SOM patterns represent conditions with moderate or strong near-surface
343 stability capped by enhanced stability aloft (-SSA, -VSSA, or -ESSA).

344 The SOM for South Pole (Figure 2) shows the boundary layer height for each SOM pattern, in
345 addition to showing potential temperature gradient and anomaly profiles. The boundary layer depth rarely
346 exceeds 100 m across the SOM and is very shallow (less than 50 m AGL) for the SS, VSS, and ESS cases
347 present throughout much of the SOM. Boundary layer depth increases in the MS cases in the bottom right
348 corner of the SOM (approximately 100 m) and is deepest in the NN and VSM cases in the top right of the
349 SOM (just above 100 m).

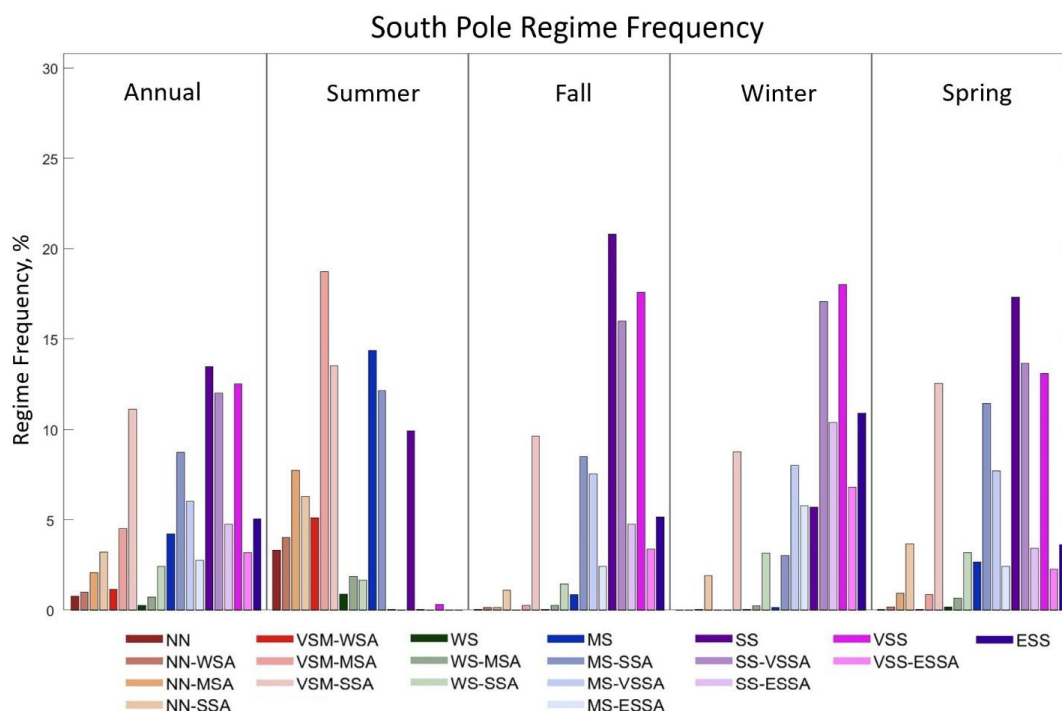


350 Figure 2: Profiles of mean potential temperature gradient (pink line, top axis), and mean potential temperature
 351 anomaly (blue line, bottom axis) calculated from the BMUs that map to each SOM pattern from 20 to 500 m above
 352 ground level at South Pole.

353 As mentioned in Section 2.2.2, the stability regime for each individual radiosonde profile was
 354 identified to allow for comparison of regime frequencies across all five sites. Annual and seasonal
 355 stability regime frequencies at South Pole are shown in Figure 3. When analyzing the frequency of
 356 boundary layer stability regimes on an annual basis (Figure 3, left panel) the strongest near-surface
 357 stability regimes (SS, VSS and ESS) are most common, occurring 58.5% of the time cumulatively. This
 358 observation is consistent with what is seen in the SOM, where most of the profiles are SS, VSS, and ESS
 359 regimes. For the weaker stability regimes (NN, VSM, and WS) the most common types of these regimes
 360 are the ones with enhanced stability aloft indicating that most of the time when weak stability is present
 361 near the surface moderate or strong stability remains aloft. Regardless of where strong stability occurs in
 362 the profile (near-surface or aloft), strong stability, very strong stability, and extremely strong stability
 363 occurs 85.1% of the time annually at the South Pole indicating that this location is dominated by the
 364 strongest stability classes.



365 Seasonally there is a clear difference in regime frequencies between summer (DJ) and the other
 366 three seasons. In the summer, the weakest near-surface stability regimes (NN and VSM) account for most
 367 summer cases (58.7%), although often with enhanced stability aloft. Despite the sun being continuously
 368 above the horizon during the summer, a high frequency of the MS and SS regimes (36.8%) still occurs.
 369 WS regimes are very rare (4.5%), along with the VSS and ESS regimes, which almost never occur at this
 370 time of year. In the winter (MJJA), SS, VSS, and ESS regimes dominate, occurring 68.9% of the time,
 371 while NN and VSM occur only 10.7% of time, and WS and MS cases make up the remainder of stability
 372 regimes observed in winter (3.4% and 16.9%, respectively). Interestingly, the few NN, VSM, and WS
 373 cases in the winter all have strong stability aloft (-SSA), indicating that even when the weakest stability
 374 regimes occur at the surface, strong stability is still present just above the boundary layer. The frequency
 375 of stability regimes in the transition seasons (fall, FMA, and spring, SON) largely mirrors the frequency
 376 of stability regimes in winter, again with the observation that the NN, VSM, and WS cases in the fall and
 377 spring almost always have strong stability aloft (-SSA).



378 *Figure 3: Percentage of observations corresponding to each boundary layer stability regime observed at South Pole*
 379 *annually (left panel) and seasonally (right 4 panels - summer, fall, winter, and spring). The regimes for the annual*
 380 *and seasonal plots are arranged with increasing stability from left to right in each panel, and the order of the*
 381 *stability regimes in each panel corresponds to the order of the regimes, from top to bottom and left to right in the*
 382 *colored key at the bottom.*

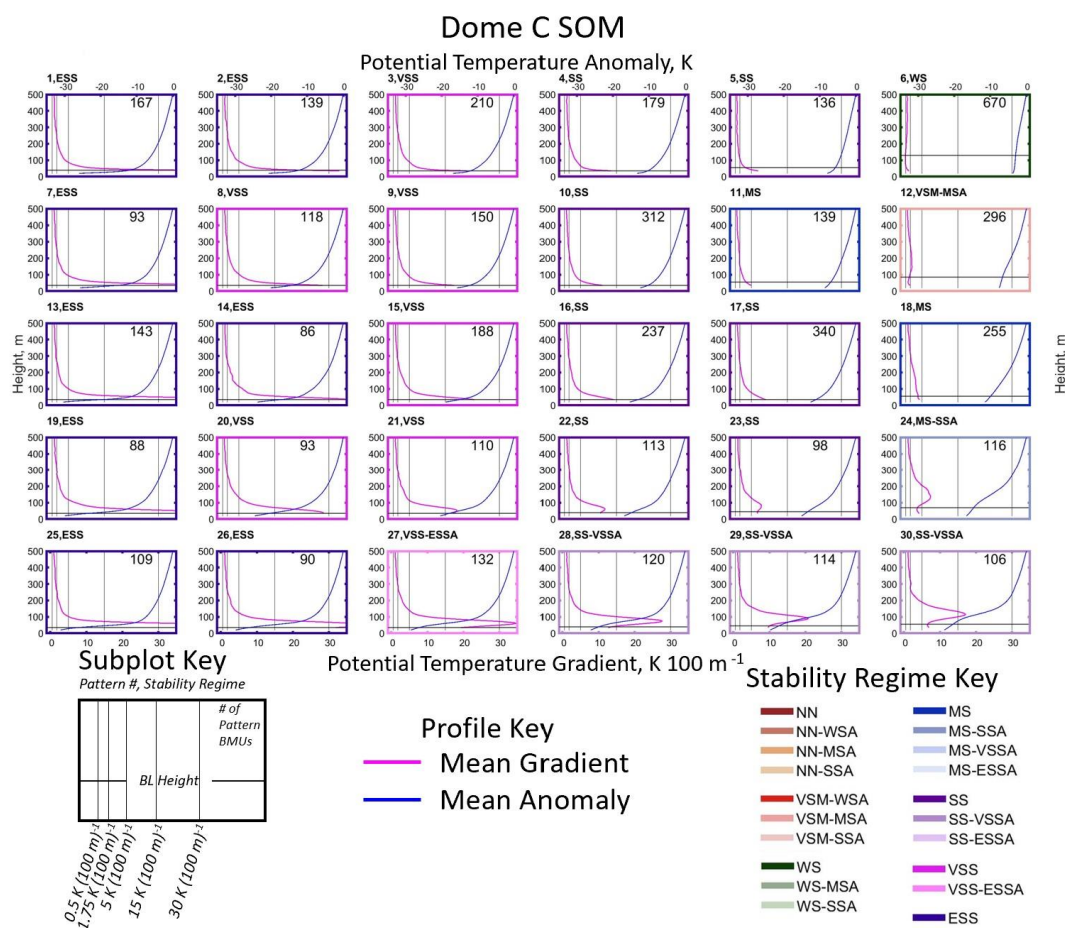
383 3.2 Dome C

384 Dome C is another high-plateau continental interior site where strong stability persists throughout
 385 much of the year (King and Turner, 1997; Andreas et al., 2000). This can be seen in the Dome C SOM in
 386 Figure 4, where, like South Pole, most of the SOM-identified profiles exhibit potential temperature



387 gradients in excess of 5 K (100 m)^{-1} , and many are greater than $15 \text{ K (100 m)}^{-1}$. The left four columns of
388 the SOM are all SS or stronger stability regimes (greater than 5 K (100 m)^{-1}), and stability decreases from
389 left to right with the weakest stability patterns in the upper right corner (less than $1.75 \text{ K (100 m)}^{-1}$). The
390 height of the maximum potential temperature gradient within the profile changes across the SOM, with
391 the maximum stability observed at the surface in the upper left profiles, and the height of this maximum
392 stability increasing to the bottom right of the SOM, although the strongest stability usually occurs near the
393 surface in most of the SOM patterns.

394 The boundary layer height is less than 50 m across most of the SOM, and only increases when
395 stability decreases, such as in the bottom right, where stability is moderate and the boundary layer height
396 is about 75 m, and in the top right, where stability is weak, and the boundary layer height is around 100
397 m. In general, these are still very shallow boundary layers, even in the weaker stability patterns, compared
398 to other locations across the planet, where the height of the boundary layer can exceed 1000 m (Stull,
399 1988). Both at South Pole and Dome C strong, near-surface stability suppresses most of the mechanically
400 generated turbulence resulting in very shallow (typically less than 75 m) boundary layers. However,
401 shallow boundary layers at both sites also occur in the upper right portions of the SOM where relatively
402 weak stability exists, indicating that near-surface turbulent mixing is still confined to the lowest part of
403 the atmosphere (less than 150 m).

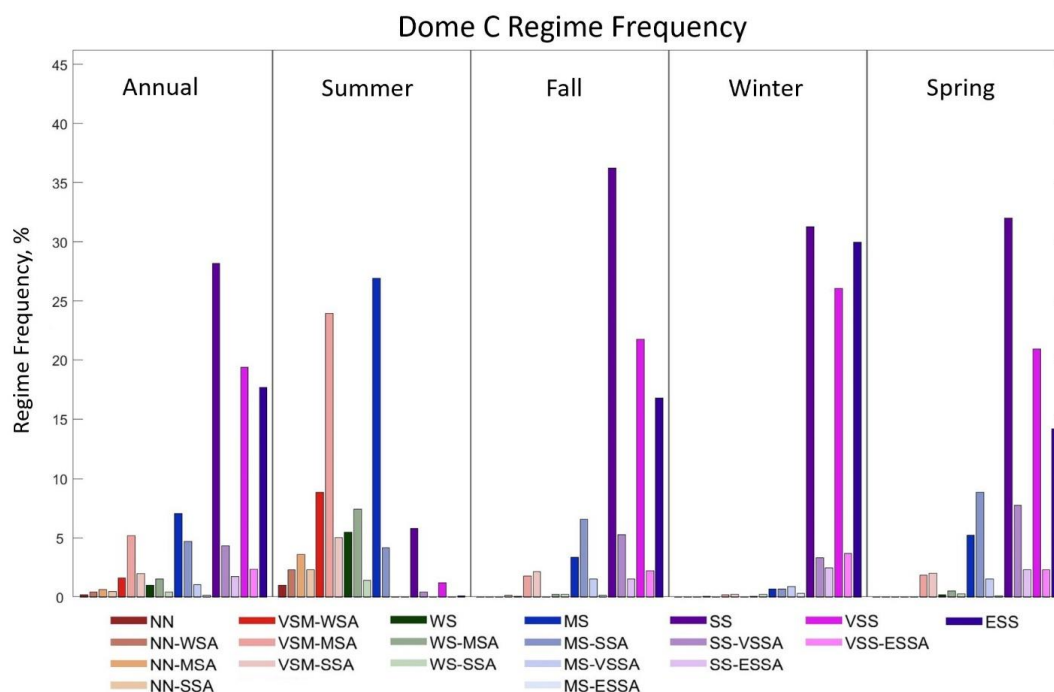


404 *Figure 4: Profiles of mean potential temperature gradient (pink line, top axis), and mean potential temperature*
 405 *anomaly (blue line, bottom axis) calculated from the BMUs that map to each SOM pattern from 20 to 500 m above*
 406 *ground level at Dome C.*

407 The frequency of occurrence of each stability regime at Dome C is shown in Figure 5. On an
 408 annual basis, SS, VSS and ESS regimes occur most frequently (73.6%), while the weaker stability
 409 regimes, NN, VSM, and WS only occur 13.5%. This is comparable to the range of stability regimes seen
 410 in the SOM, where these types of weaker stability regimes occur very rarely, and SS, VSS, and ESS
 411 regimes dominate across most of the SOM. A strong seasonal cycle emerges, with the weaker stability
 412 regimes dominant in summer and the strongest stability regimes dominant in winter. The summer season
 413 is largely characterized by NN, VSM, and WS regimes (61.4%), as well as MS regimes (31.1%). In the
 414 summer, SS, VSS, and ESS regimes occur only 7.5% of the time, indicating the rarity of strong stability
 415 at this time of year. In the winter, SS, VSS, and ESS regimes occur almost exclusively (96.7%), while all
 416 the other regime groupings (VSM, NN, WS, and MS) occur very rarely (3.3%). It is also interesting that
 417 the dominant regimes in the winter are solely the basic near-surface stability regimes of SS, VSS, and
 418 ESS regimes, and increased stability aloft in these regimes occurs much less frequently indicating that
 419 during the winter the strongest stability occurs at the surface most of the time, with infrequent cases of
 420 weakened stability near the surface and enhanced stability aloft. The frequency of stability regimes in the



421 transition seasons (fall and spring) is also dominated by stronger stability regimes (SS, VSS and ESS),
 422 although with slightly lower frequencies than in winter, with these regimes occurring 83.7% and 76.9% of
 423 the time in fall and spring respectively. The weakest stability regimes (VSM, NN, and WS) occur rarely
 424 (4.6% and 4.9% of the time in fall and spring, respectively), while the MS regime occurs 11.7% and
 425 15.7% of the time in fall and spring, respectively. In comparison to the summer and winter, the transition
 426 seasons behave more like the winter season when it comes to regime frequency, with most regimes being
 427 strong stability.



428 *Figure 5: Percentage of observations corresponding to each boundary layer stability regime observed at Dome C*
 429 *annually (left panel) and seasonally (right 4 panels - summer, fall, winter, and spring). The regimes for the annual*
 430 *and seasonal plots are arranged with increasing stability from left to right in each panel, and the order of the*
 431 *stability regimes in each panel corresponds to the order of the regimes, from top to bottom and left to right in the*
 432 *colored key at the bottom.*

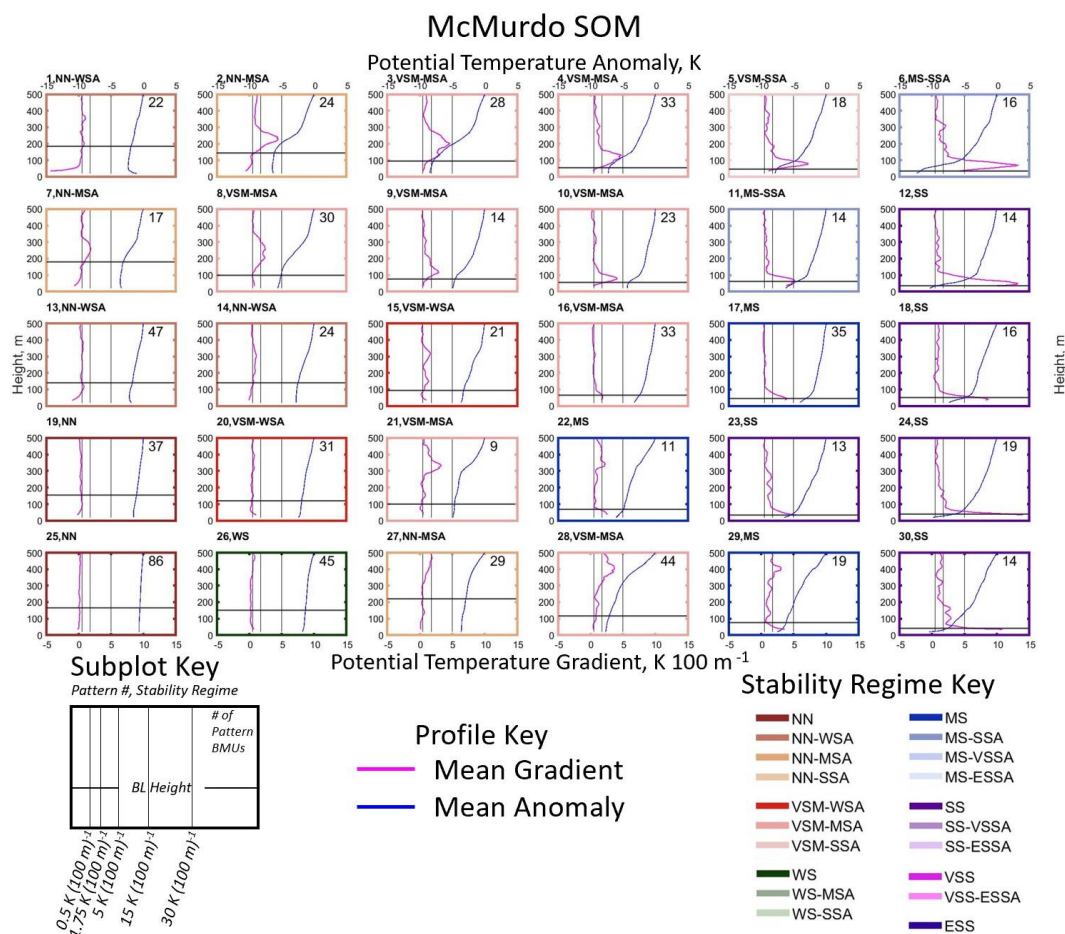
433 3.3 McMurdo

434 So far, two continental interior sites, South Pole and Dome C have been analyzed, and now the
 435 coastal sites, McMurdo, Neumayer, and Syowa will be analyzed. In comparison to the continental
 436 interior, coastal locations are more exposed to the impacts of cyclonic activity, increased cloud cover and
 437 moisture, as well as warmer surface temperatures and weaker inversions (Phillpot and Zillman, 1970;
 438 Cassano et al., 2016). Given these previous observations, it is expected that weaker stability will be
 439 present at the coastal sites compared to the near-constant state of strong stability observed at the colder,
 440 continental interior sites described above.

441 Stability profiles at McMurdo identified by the SOM span a range from NN to SS regimes, as
 442 seen in Figure 6. Stability in the SOM increases from left to right, with the weakest stability patterns in



443 the top left and strongest stability patterns in the bottom right. In addition to this gradient in stability
 444 across the SOM the height of the strongest stability increases from the surface in the bottom rows of the
 445 SOM to above a near surface layer of weaker stability in the top middle of the SOM. Most of these
 446 patterns with enhanced stability aloft exhibit moderate or strong stability (-MSA or -SSA, respectively)
 447 above a layer of weaker stability. Two-thirds of the SOM patterns exhibit potential temperature gradients
 448 less than $1.75 \text{ K } (100 \text{ m})^{-1}$, corresponding to WS or weaker stability, and only five patterns on the right
 449 side of the SOM (patterns 12, 18, 23, 24, and 30) exhibit strong stability with gradients greater than $5 \text{ K } (100 \text{ m})^{-1}$.
 450 It can also be seen that the height of the boundary layer increases from the bottom right
 451 (approximately 50 m) to the top left (approximately 200 m), as stability decreases, and the height of the
 452 maximum stability increases in the profile.

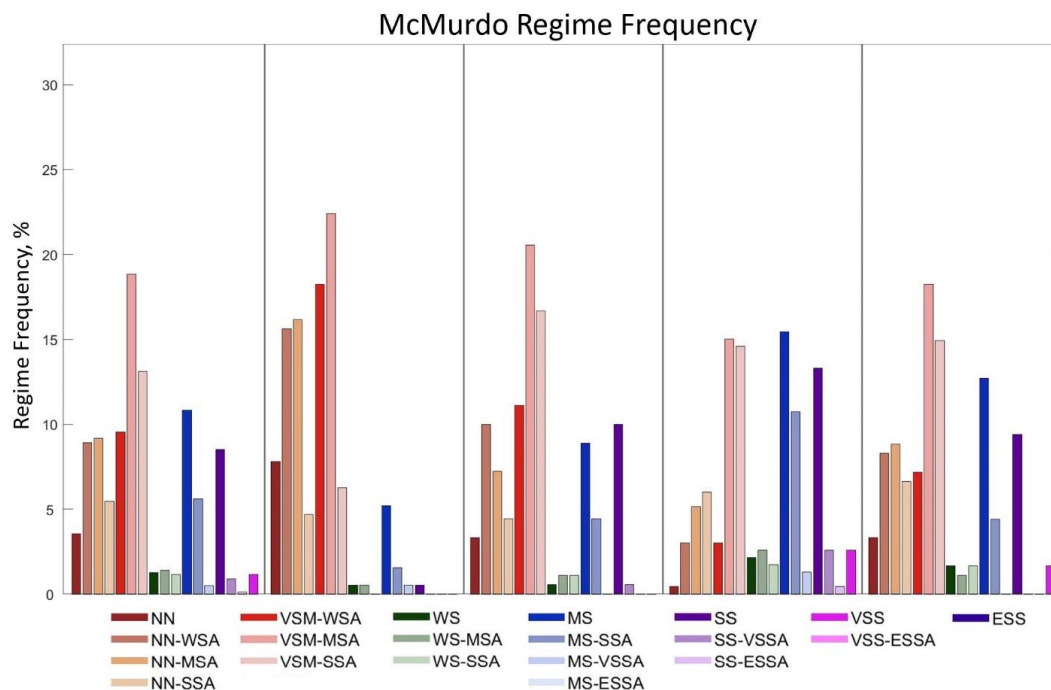


453 *Figure 6: Profiles of mean potential temperature gradient (pink line, top axis), and mean potential temperature*
 454 *anomaly (blue line, bottom axis) calculated from the BMUs that map to each SOM pattern from 20 to 500 m above*
 455 *ground level at McMurdo.*

456 Considering regime frequencies on an annual basis the NN and VSM regimes are most common
 457 (68.6 %), followed by MS and SS regimes (24.9 %). The summer season is dominated by NN and VSM
 458 regimes (91.2%), and WS, MS, and SS regimes occur only 8.8% of the time. This distribution of stability



459 is consistent with increased radiative forcing and previous observations of weaker stability in summer
 460 compared to other seasons at a site approximately 100 km from McMurdo (Cassano et al., 2016). In the
 461 winter, when it would be expected that strong stability would be dominant, only about half of the time
 462 regimes with stability MS and greater occur (46.4%) while regimes with stability WS and weaker occur
 463 just over half of the time (53.6%). However, when the regimes with stability WS and weaker occur,
 464 moderate or strong stability aloft (-MSA and -SSA, respectively) is usually present (84% of NN, VSM,
 465 and WS cases have -MSA or -SSA), indicating that even when weaker stability occurs near the surface
 466 moderate or stronger stability is present just above the boundary layer. In the transition seasons, MS and
 467 stronger cases occur 23.9% of the time in the fall and 28.2% of the time in the spring. NN and VSM cases
 468 cumulatively occur 73.3% of the time in fall and 67.3% in the spring, while WS cases are largely absent.
 469 In the VSM regime grouping, the -MSA and -SSA regimes are most common with the -WSA regime
 470 occurring less frequently in comparison in both spring and fall. In the NN regime grouping, the frequency
 471 of occurrence decreases with increasing stability aloft in the fall, and is more consistent across the -WSA,
 472 -MSA, and -SSA regimes in the spring. This indicates that in the fall, it is more common for NN cases to
 473 have weak rather than strong stability aloft, like what was observed in the summer, and opposite that in
 474 the winter.

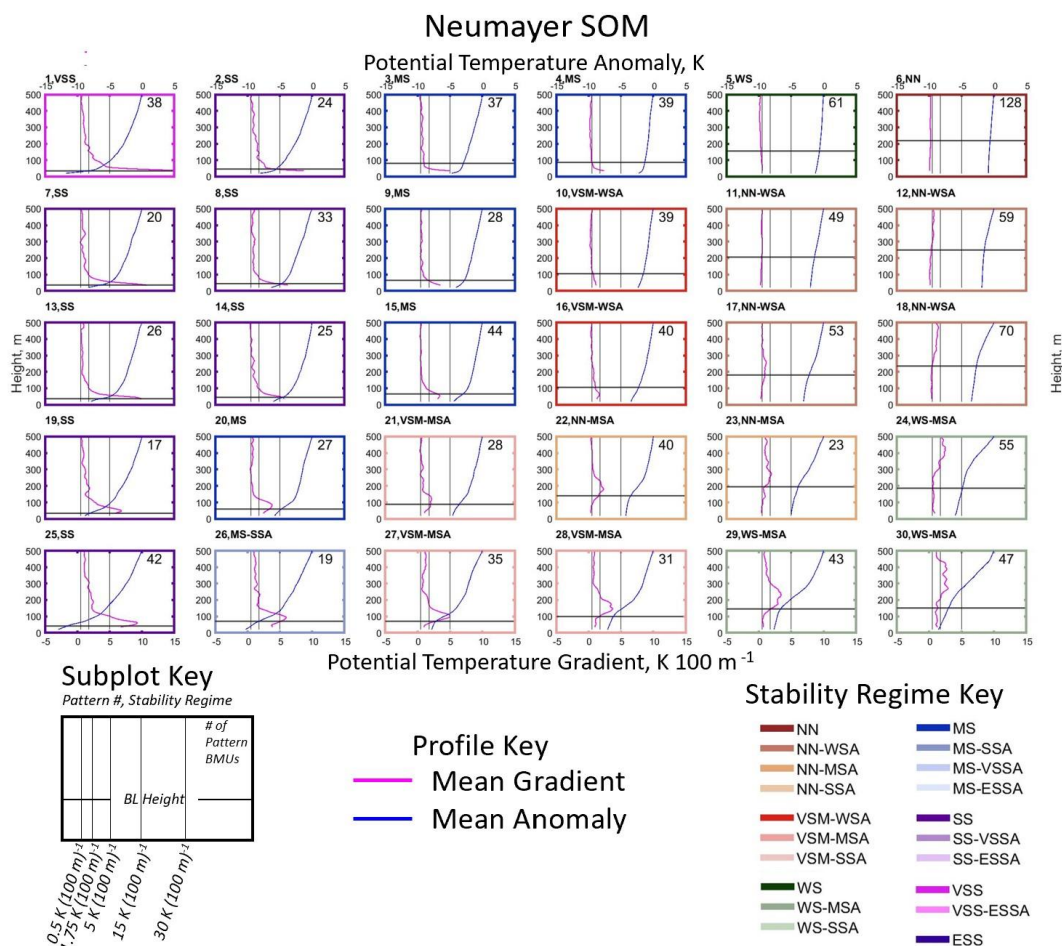


475 *Figure 7: Percentage of observations corresponding to each boundary layer stability regime observed at McMurdo*
 476 *annually (left panel) and seasonally (right 4 panels - summer, fall, winter, and spring). The regimes for the annual*
 477 *and seasonal plots are arranged with increasing stability from left to right in each panel, and the order of the*
 478 *stability regimes in each panel corresponds to the order of the regimes, from top to bottom and left to right in the*
 479 *colored key at the bottom.*



480 **3.4 Neumayer**

481 Neumayer is a coastal site located near sea-level, heavily influenced by large-scale cyclonic
482 activity (Silva et al., 2022), and where the proximity of sea ice and open ocean can affect boundary layer
483 stability throughout the year (Silva et al., 2022). Stability regimes at Neumayer span a range from NN to
484 VSS regimes, as seen in the SOM in Figure 8. Generally, stability decreases from left to right across the
485 SOM. Stability on the left side of the SOM decreases from the top to the bottom of the SOM, with the
486 strongest stability regimes in the top left. On the right side of the SOM deep near neutral or weak stability
487 patterns occur at the top of the SOM with patterns characterized by increasing stability aloft occurring
488 towards the bottom of the SOM. This SOM shows two general modes of stability split by a bottom left to
489 top right diagonal, with the portion to the right of this diagonal characterized by NN, VSM, and WS
490 regimes, and the portion to the left characterized by MS, SS, and VSS regimes. The boundary layer height
491 at Neumayer increases from the left side of the SOM, where very shallow boundary layers exist (less than
492 50 m) with strong stability, to the top right, where the boundary layer height increases to above 200 m.

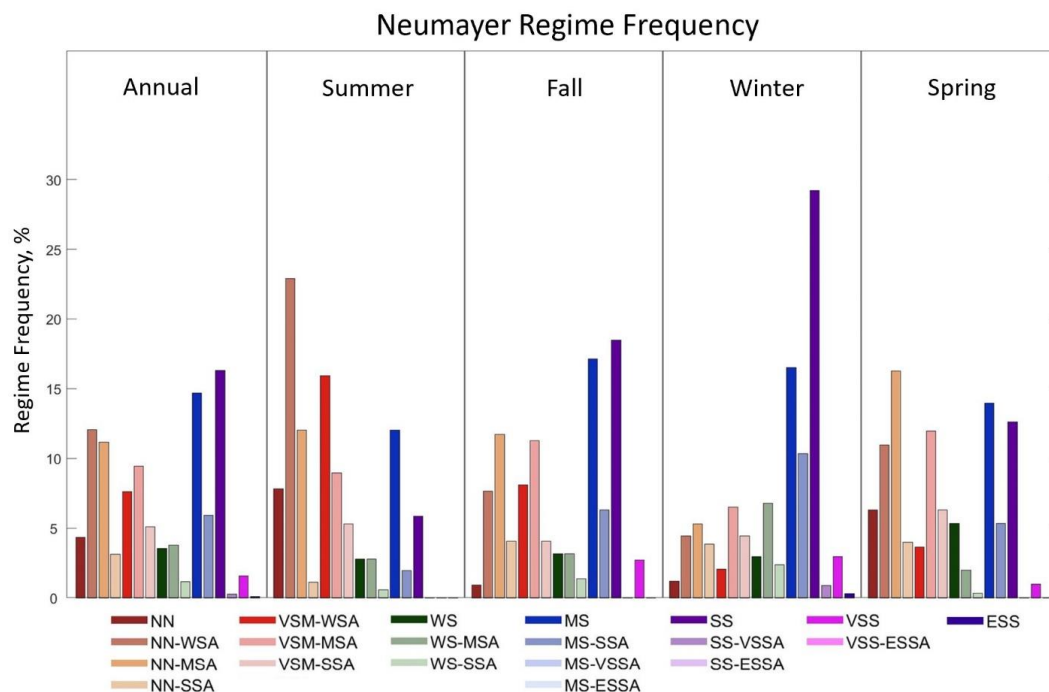


493 Figure 8: Profiles of mean potential temperature gradient (pink line, top axis), and mean potential temperature
 494 anomaly (blue line, bottom axis) calculated from the BMUs that map to each SOM pattern from 20 to 500 m above
 495 ground level at Neumayer.

496 On an annual basis, the NN and VSM regime groupings are most common (52.8%), and the MS
 497 and SS (37.2%) regimes occur slightly less frequently at Neumayer (Figure 9). The WS regime grouping
 498 occurs 8.4% while VSS and ESS regimes are rare and occur only 1.6% of the time throughout the year.
 499 The summer season is dominated by NN and VSM regimes (74%). WS (6.1%), MS (14%), and SS
 500 (5.9%) regimes are much less common in comparison. In the VSM and NN regime groupings regimes
 501 with weak stability aloft (-WSA) are more common than those with stronger stability aloft (-MSA and -
 502 SSA). In the winter, regimes with MS or greater stability are most common (60.1%), while regimes with
 503 weaker stability, WS (12.2%), VSM (13%), and NN (14.7%), occur less frequently. Further, many of the
 504 weaker stability regimes present in the winter are those with increased stability aloft, especially -MSA
 505 and -SSA, indicating that moderate or stronger stability is frequently present either near the surface or
 506 aloft in winter (89.5% of the time), whereas in the summer these moderate or strong stability cases (either
 507 at the surface or aloft) cumulatively occur 50.7% of the time. In the fall, NN and VSM cases (47.9%) and
 508 MS and stronger cases (44.6%) occur with almost equal frequency, unlike in the summer when the NN



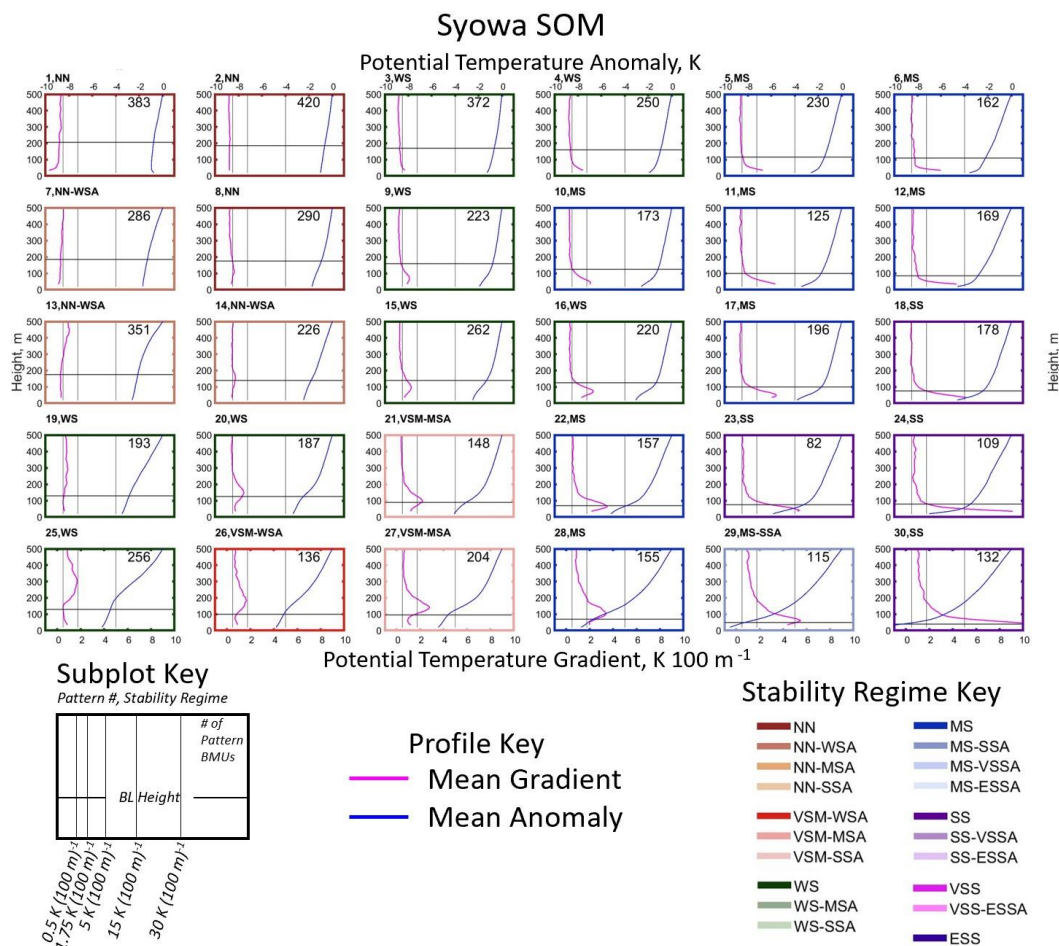
509 and VSM cases are dominant, and winter when the MS and stronger cases are dominant. In the spring, the
 510 VSM and NN cases (59.6%) occur more frequently than the MS and stronger cases (32.9%), which is
 511 more similar to the distribution of regimes in the summer, when weaker stability regimes dominate.



512 *Figure 9: Percentage of observations corresponding to each boundary layer stability regime observed at Neumayer*
 513 *annually (left panel) and seasonally (right 4 panels - summer, fall, winter, and spring). The regimes for the annual*
 514 *and seasonal plots are arranged with increasing stability from left to right in each panel, and the order of the*
 515 *stability regimes in each panel corresponds to the order of the regimes, from top to bottom and left to right in the*
 516 *colored key at the bottom.*

517 3.5 Syowa

518 Syowa is a coastal site near sea-level, impacted cyclonic activity and by katabatic winds from the
 519 continental interior (Murakoshi, 1958), which sometimes result in strong wind events (Yamada and
 520 Hirasawa, 2018). Stability at Syowa spans a range from NN (top left corner of SOM) to SS (bottom right
 521 corner of SOM) regimes, as seen in the SOM in Figure 10. Stability generally increases from left to right
 522 and top to bottom across the SOM. The height of the maximum potential temperature gradient is near the
 523 surface on the far-right side of the SOM and increases to approximately 300 m in the bottom left. Shallow
 524 boundary layers associated with the strong stability patterns in the bottom right increase in height to the
 525 top left, where near-neutral conditions extend through a deeper, 200 m boundary layer.

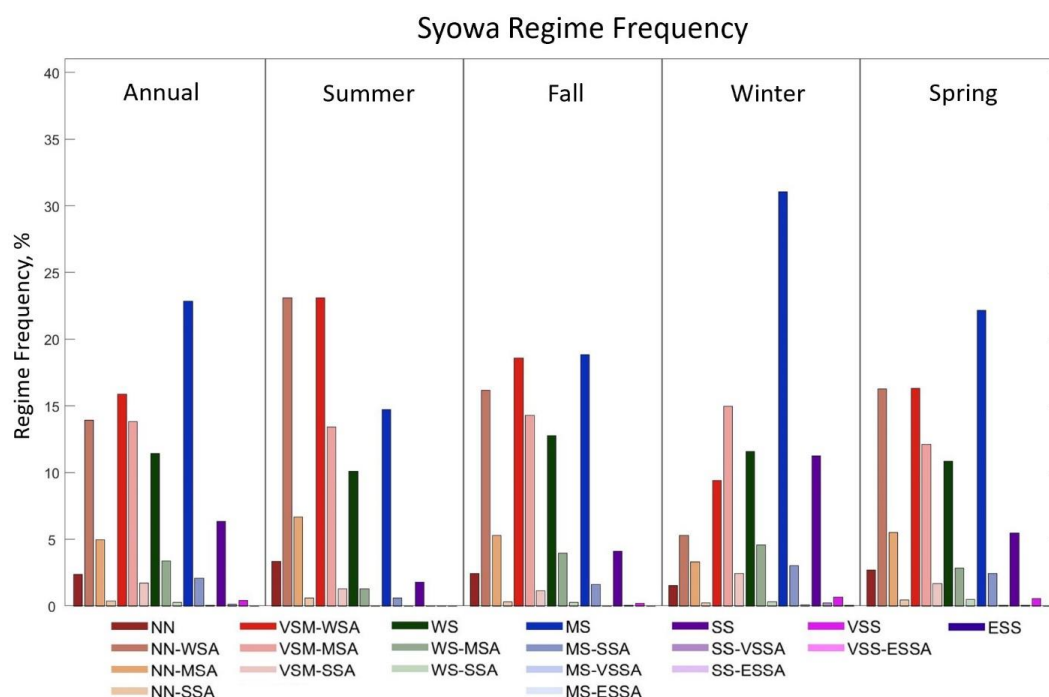


526 *Figure 10: Profiles of mean potential temperature gradient (pink line, top axis), and mean potential temperature*
 527 *anomaly (blue line, bottom axis) calculated from the BMUs that map to each SOM pattern from 20 to 500 m above*
 528 *ground level at Syowa.*

529 The frequency of occurrence of each stability regime at Syowa, annually and seasonally, is shown
 530 in Figure 11. On an annual basis, a mix of regimes are observed, mostly in the NN (21.8%) and VSM
 531 (31.4%) regime groupings, with enhanced stability aloft common. The WS regime (15.1%) and MS
 532 regime (25.1%) also occur frequently, on an annual basis, but enhanced stability aloft rarely occurs in
 533 these regime groupings. The strongest stability regimes (SS, VSS and ESS) occur infrequently (6.8%).
 534 These results indicate that near neutral to moderate stability is most common at Syowa, while stronger
 535 stability is rare. The summer season is dominated by the NN and VSM regimes (71.5%), while the WS
 536 regime occurs 11.4% of the time, and the MS regime 15.3% of the time. In all regime groupings in the
 537 summer, strong stability aloft (-SSA) regimes are less common than weak or moderate stability aloft (-
 538 WSA and -MSA, respectively), which is reflective of the lack of strong stability regimes in general in this
 539 season. In the winter, MS and SS regimes (45.4%) occur about as often as the NN and WS regimes
 540 (43.4%), but MS is by far the most common individual regime in winter (31%). Regimes with increased
 541 stability aloft (-MSA and -SSA) are uncommon in the winter except in the VSM regime grouping, and



542 rather the basic near-surface stability regimes (without enhanced stability aloft) or -WSA cases are more
 543 common. In the transition seasons, a variety of regimes occur with similar frequencies. In the fall the most
 544 common regime groupings are the VSM cases (34%) followed by the NN cases (24.2%) and the MS cases
 545 (20.4%), and in the spring, the VSM (30.5%) regimes are most common followed by MS (24.6%), and
 546 NN (24.5%) regimes that occur with nearly identical frequencies. In both seasons, like the summer and
 547 winter, -MSA and -SSA cases occur rarely, with -WSA being more common when increased stability
 548 aloft is observed for a given regime grouping.



549 *Figure 11: Percentage of observations corresponding to each boundary layer stability regime observed at Syowa*
 550 *annually (left panel) and seasonally (right 4 panels - summer, fall, winter, and spring). The regimes for the annual*
 551 *and seasonal plots are arranged with increasing stability from left to right in each panel, and the order of the*
 552 *stability regimes in each panel corresponds to the order of the regimes, from top to bottom and left to right in the*
 553 *colored key at the bottom.*

554 3.6 Stability Regime Frequencies for Clear and Cloudy Conditions

555 As discussed in the introduction and methods, stability in the polar boundary layer is often
 556 described in the literature as a two-regime system, with cloudy states characterized by large values of
 557 downwelling longwave radiation and weak stability and clear states characterized by small values of
 558 downwelling longwave radiation and strong stability (Mahrt et al., 1998; Mahrt, 2014; Solomon et al.,
 559 2023). To determine if this two-regime description of boundary layer stability and cloud cover is observed
 560 in the Antarctic a clear or cloudy attribution was given to each radiosonde profile based on the surface net
 561 longwave radiation value at the time of launch following the method described in Section 2.2.3, based on
 562 Solomon et al. (2023).

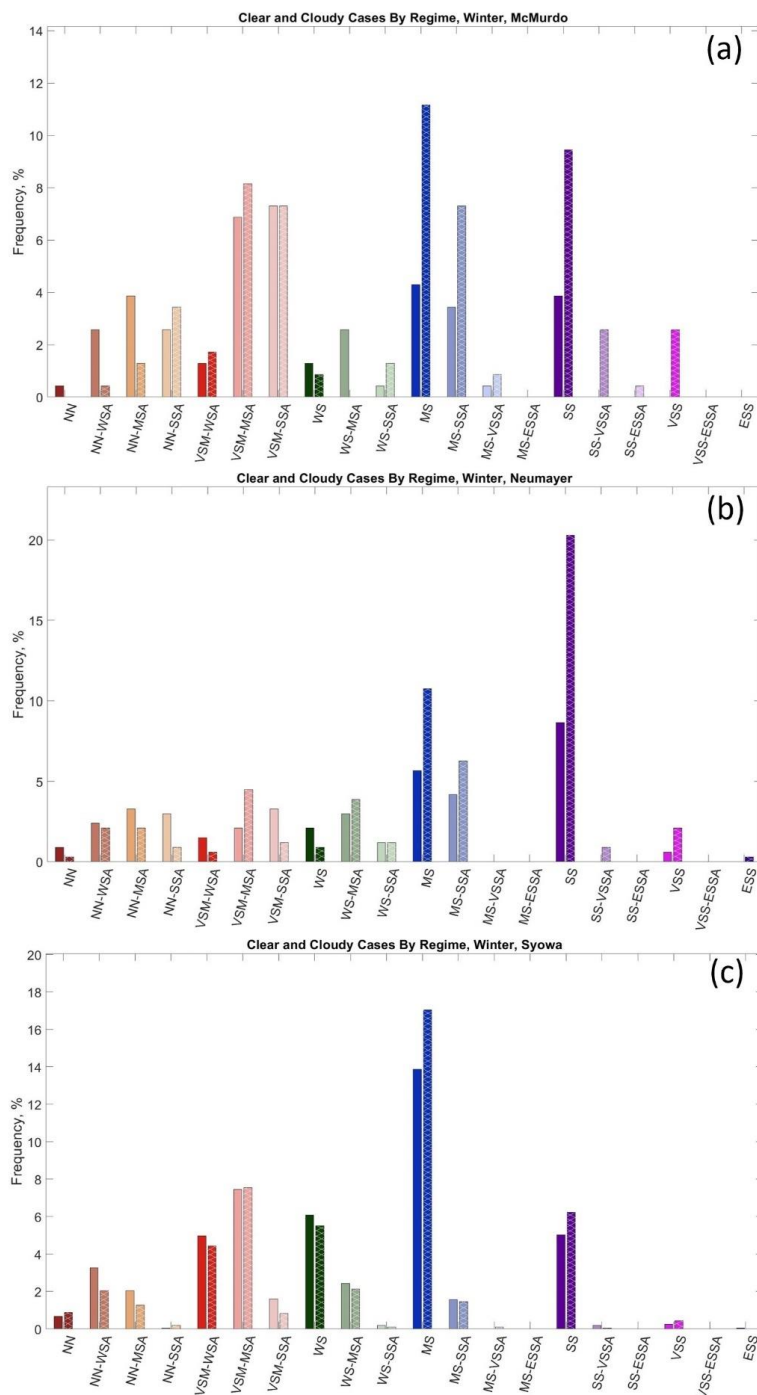


563 Solomon et al. (2023) found that the difference between cloudy and clear states in the Arctic
564 could be defined by a threshold value of net longwave radiation marking the minimum in the PDF
565 between two peaks in a bimodal distribution of net longwave radiation. PDFs of winter net longwave
566 radiation at the five Antarctic sites analyzed in this paper are shown in Figures S1 to S5. The PDFs for the
567 two interior sites (Dome C and South Pole, Figures S1 and S2) do not show a bimodal distribution while
568 the three coastal sites do (Figures S3 to S5). The overlap ratio for the cloudy and clear downwelling
569 longwave radiation PDFs for each site, as described in Section 2.2.3, further support the lack of distinct
570 cloudy and clear radiative states at the interior sites, with large values of this ratio (0.84 at South Pole and
571 0.91 at Dome C) indicating that there is no value of net longwave radiation that allows a meaningful
572 separation between cloudy and clear states with unique distributions of downwelling longwave radiation.
573 In contrast, the three coastal sites have overlap ratios of less than 0.5 (0.19 for McMurdo, 0.33 for
574 Neumayer, and 0.46 for Syowa) for net longwave radiation threshold values that correspond closely to the
575 minimum in the net longwave radiation PDF (Figures S3 to S5), indicating that distinct downwelling
576 longwave radiation distributions exist for cloudy and clear states at these sites. As such, we will evaluate
577 the frequency of stability regimes for cloudy and clear conditions at the three coastal sites, but not for the
578 interior sites.

579 Figure 12 shows the frequency of each stability regime for cloudy (solid bars) and clear (hatched
580 bars) cases for the three coastal sites: McMurdo, Neumayer, and Syowa. At McMurdo (Figure 12a), the
581 most obvious result is that in the MS, SS, and VSS regimes occur much more frequently during the clear
582 sky state. This result is consistent with previous observations that clear skies allow for radiative cooling
583 and the development of strong near surface stability (Stone and Kahl, 1991; Hudson and Brandt, 2005). In
584 contrast, the NN and WS regimes generally occur preferentially during cloudy conditions, also consistent
585 with previous results that increased cloud cover reduces near-surface stability (Stone and Kahl, 1991;
586 Hudson and Brandt, 2005). Interestingly, the VSM and NN-SSA regimes occur nearly equally regardless
587 of cloud cover. This indicates that changes in downwelling longwave radiation related to varying cloud
588 cover do not play a dominant role in the forcing of these regimes.

589 When examining the distribution for Neumayer (Figure 12b), the SS regime is over twice as
590 frequent during clear compared to cloudy conditions, as expected (Stone and Kahl, 1991; Mahrt et al.,
591 1998; Mahrt, 2014; Solomon et al., 2023). The same is true for the VSS regime, and clear conditions are
592 present for the singular ESS regime as well. The MS and MS-SSA regimes also occur more frequently
593 with clear rather than cloudy conditions. The NN regimes usually occur with cloudy compared to clear
594 conditions. The various VSM and WS regimes have occurrences where sometimes clear, and sometimes
595 cloudy, periods are dominant. There are also VSM and WS regimes where they are roughly equal. This
596 suggests that changes in downwelling longwave associated with changes in cloud cover do not play a
597 primary role in forcing the VSM or WS regimes to occur.

598 Finally, at Syowa (Figure 12c), an interesting pattern emerges, where the frequency of most
599 stability regimes is similar for both cloudy and clear conditions. This is surprising, given that previous
600 studies have found weaker stability is favored by cloudy conditions, and stronger stability is favored by
601 clear conditions. This is not the case at Syowa, and may indicate that changes in downwelling longwave
602 radiation, associated with cloudy and clear conditions, do not exert a strong control on near surface
603 stability at this site.



604 Figure 12: The distribution of the various boundary layer stability regimes at McMurdo (a), Neumayer (b), and
 605 Syowa (c) split into cloudy (left, solid bars) clear (right, hatched) observations in the winter season.



606 4 Discussion and Conclusions

607 SOMs have been used in the results presented above to identify the range of boundary layer
608 stability profiles at two continental interior and three coastal Antarctic sites (Figures 2, 4, 6, 8 and 10).
609 Based on the SOM analysis a quantitative boundary layer stability definition was developed and applied
610 to classify the SOM patterns into unique stability regimes. While several studies have examined general
611 trends in boundary layer stability at individual sites in Antarctica (Hudson and Brandt, 2005; Cassano et
612 al., 2016; Silva et al., 2022), or estimated inversion strength empirically (Phillpot and Zillman, 1970), no
613 known study has completed a widespread comparison of the range and seasonality of boundary layer
614 stability across the continent.

615 The stability regimes present, and frequency of these regimes, differed between the continental
616 interior sites and the coastal sites. At the interior sites, South Pole and Dome C, strong stability patterns
617 dominate the SOM consistent with previous studies of near-surface stability on the polar plateau (Hudson
618 and Brandt, 2005; King and Turner, 1997; Andreas et al., 2000). Twenty seven of 30 patterns at South
619 Pole (Figure 2) and 28 of 30 at Dome C (Figure 4) have stability between MS and ESS, with potential
620 temperature gradients in excess of $30 \text{ K (100 m)}^{-1}$ in several of the SOM profiles. Some of the SOM-
621 identified profiles at these sites have weaker stability near the surface, with stronger stability aloft, and
622 these patterns are more common at South Pole (Figure 2, bottom two rows) than at Dome C (Figure 4,
623 bottom right corner). Finally, there are generally more VSS and ESS patterns in the Dome C SOM (left
624 two columns) compared to the South Pole SOM (upper left corner), indicating stronger stability at this
625 site, which was also observed by Hudson and Brandt (2005).

626 In contrast to the interior sites, at the coastal sites, McMurdo (Figure 6), Neumayer (Figure 8),
627 and Syowa (Figure 10), the SOM profiles are more evenly distributed across NN, VSM, WS, MS, and SS
628 profiles with only one VSS profile and no ESS profiles. Across all three coastal sites, over half of the
629 SOM-identified patterns have a potential temperature gradient less than $1.75 \text{ K (100 m)}^{-1}$. These gradients
630 occurred for only two or three patterns at Dome C and South Pole, respectively. This indicates more
631 favorable conditions for weaker near-surface stability at coastal sites (Phillpot and Zillman, 1970;
632 Cassano et al., 2016). This clearly distinguishes the boundary layer conditions of the continental interior
633 sites from those at the coastal sites, as also noted by Lettau and Schwerdtfeger, (1967), Phillpot and
634 Zillman, (1970), Comiso, (1994), Zhang, et al. (2011), and Cassano et al. (2016). It is also important to
635 note the common occurrence of enhanced stability above a layer of weaker near-surface stability in the
636 SOMs for the coastal sites in comparison to the continental interior sites. This phenomenon rarely occurs
637 in the Dome C SOM, only in the bottom right corner (Figure 4), and across the bottom two rows in the
638 South Pole SOM (Figure 2), but across much of the SOMs for McMurdo (Figure 6) and Neumayer
639 (Figure 8), and some of the SOM for Syowa as well (Figure 10).

640 The SOM analysis indicates a mean boundary layer depth being much shallower at Dome C (45
641 m) and South Pole (60 m) compared to the coastal sites (95 m to 120 m). The strong near-surface stability
642 that is almost always present at the continental interior sites limits the depth and strength of turbulent
643 mixing, while weaker stability at the coastal sites allows for stronger near-surface turbulence and thus
644 increased boundary layer depths. This behavior of boundary layer depth is also observed by King and
645 Turner (1997), who found shallow boundary layers in the continental interior with boundary layer depth
646 increasing towards the coasts. Pietroni et al. (2012) estimated the wintertime boundary layer height at
647 Dome C using the bulk Richardson number and found it to be always below 150 m, but usually less than
648 50 m, and Aristidi et al. (2005) found shallower boundary layer depths at Dome C (less than 50 m)
649 compared to South Pole, consistent with our results.



650 To further summarize and compare the frequency of occurrence of boundary layer regimes
651 (defined in Table 2) across the Antarctic continent, Figure 13 and Table S1 provide a summary of the
652 annual and seasonal characteristics of the near-surface stability and maximum stability below 500 m
653 across all sites. Figure 13 shows the frequency of the near-surface stability regime groupings (e.g., all
654 NN, regardless of aloft stability, all VSM, regardless of aloft stability, etc.) and the maximum stability
655 present in the entire profile, either near surface or above the boundary layer and below 500 m (e.g., the
656 frequency of the basic near-surface stability regime WS and all -WSA cases, all the MS and -MSA, cases,
657 etc.). Table S1 lists the frequency of WS and weaker, MS and stronger, and SS and stronger stability near
658 the surface and for the strongest stability below 500 m.

659 Somewhat surprisingly, regimes with near-surface stability WS and weaker (Table S1) are the
660 most common regimes at the interior sites in summer (63.2% of the time at South Pole and 61.4% of the
661 time at Dome C; Figure 13c, Table S1). However, this weaker near-surface stability is often capped by
662 stronger stability above the boundary layer, such that when considering the maximum stability below 500
663 m, regimes with stability MS and stronger occur 86.7% of the time at South Pole and 81.9% of the time at
664 Dome C. This indicates that moderate or stronger stability dominates aloft even though weaker stability
665 occurs most of the time near the surface in the summer. This observation of enhanced stability above a
666 weakly stable boundary layer has not been widely documented, much less quantified, especially in the
667 continental interior of Antarctica. While winter at Dome C is characterized almost entirely by near-
668 surface stability regimes SS and stronger (96.9%), the winter at South Pole experiences these regimes less
669 often (68.8%; Figure 13g). However, when considering the maximum stability below 500 m (Figure 13h),
670 this reduced frequency of strong stability near the surface at South Pole compared to Dome C vanishes
671 and regimes with stability SS and stronger occur nearly continuously and with similar frequency at both
672 South Pole and Dome C (99.6% and 99.2% of the time, respectively; Table S1).

673 Across all three coastal sites, WS and weaker near surface stability occurs more than 50% of the
674 time in all seasons, except for Neumayer in winter (Table S1). In the summer WS and weaker near
675 surface stability is dominant, occurring 80.1% to 92.1% of the time (Figure 13c, Table S1). However, this
676 high frequency of WS or weaker stability near the surface is not evident when stability aloft is considered
677 and WS and weaker stability anywhere below 500 m occurs 42.1 to 59.6% of the time (Figure 13d, Table
678 S1). This indicates that while weaker near-surface stability is dominant in the summer at the coastal sites,
679 MS or stronger stability is nearly as frequent as WS or weaker stability above the boundary layer. In the
680 winter, WS and weaker near surface stability occurs 40% to 53.6% of the time (Figure 13g, Table S1)
681 indicating a near even split between near neutral to weak stability and moderate or stronger stability near
682 the surface. In contrast, MS and stronger stability is observed within the lowest 500 m 72.1% to 91.6% of
683 the time during the winter (Figure 13h, Table S1), indicating that weak near surface stability regimes
684 usually have enhanced (MS or stronger) stability aloft. At McMurdo, the existence of enhanced stability
685 above a layer of weaker stability was noted by Dice and Cassano (2022). Additionally, Silva et al. (2022)
686 described the boundary layer at Neumayer ranging from strong surface-based temperature inversions to
687 weak inversions near the surface with stronger inversions aloft throughout the year, which is also
688 observed here. While both Dice and Cassano (2022) and Silva et al. (2022) noted the presence of
689 enhanced stability above a layer of weaker stability, neither of these studies quantified the occurrence or
690 seasonality of this phenomenon.

691 Comparing the coastal to the continental sites, near-surface WS and weaker stability regimes are
692 much more common at the coastal sites (61.3% to 72.4%) compared to the continental interior sites
693 (13.5% to 27.2%) on an annual basis (Table S1). When considering the maximum stability below 500 m
694 MS and stronger stability occurs nearly all of the time at the interior sites (96.5 to 96.7% of the time) and

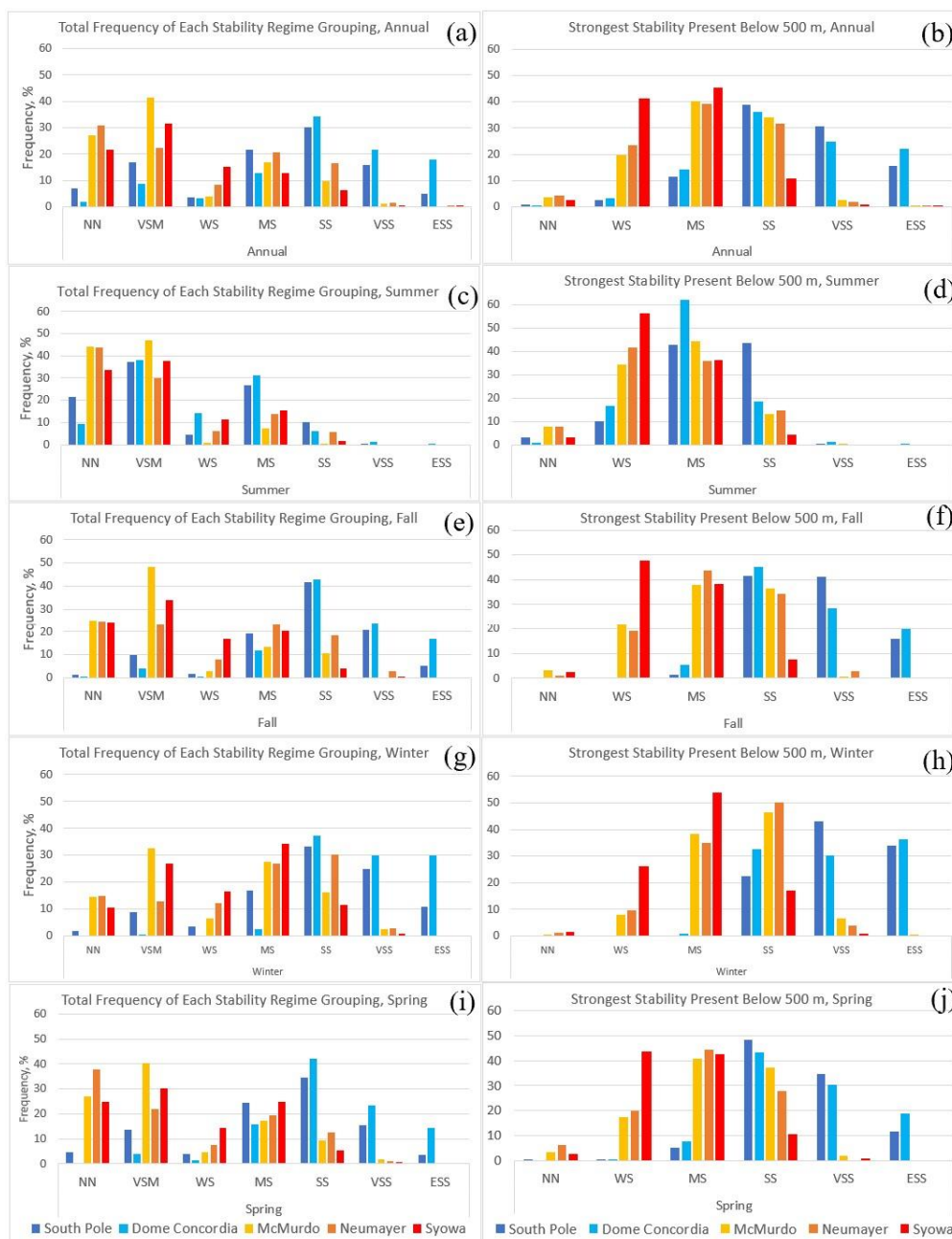


695 occurs more than half of the time at the coastal sites (56.5% to 76.6% of the time) annually (Table S1).
696 This is consistent with observations from Zhang et al. (2011) who found that surface-based temperature
697 inversions are less common along the coasts, as the coastal region is warmer, moister, and windier than
698 the continental interior, which all reduces near-surface stability.

699 In the summer, near-surface stability of WS or weaker occurs most of the time at all sites but is
700 more frequent at the coastal (80.1% to 92.1% of the time) compared to the continental sites (61.4% to
701 63.2% of the time) (Table S1). In comparison, near-surface stability regimes SS and stronger only occur
702 0.5% to 5.9% of the time at the coastal and 7.5% to 10.3% of the time at the interior sites, indicating the
703 rarity of strong near surface stability at both coastal and interior sites in the summer. However, when also
704 considering stability just above the boundary layer MS and stronger stability occurs more than 80% of the
705 time at both South Pole and Dome C (Table S1). Even at the coastal sites, MS and stronger stability
706 occurs nearly half of the time (40.4 to 57.9%) in the summer (Table S1). These results highlight that
707 while weak stability is usually present near the surface across the Antarctic continent in the summer,
708 moderate or stronger stability is often present somewhere in the lowest 500 m of the atmosphere.

709 In the winter, strong stability is expected to be dominant across Antarctica (Lettau and
710 Schwerdtfeger, 1967; Phillipot and Zillman, 1970; King and Turner, 1997; Andreas et al., 2000).
711 Surprisingly, the near-surface stability of WS and weaker still occurs 40.0% to 53.6% of the time in the
712 winter at the coastal sites, whereas these regimes, as expected, are infrequent at the interior sites,
713 occurring 14.1% of the time at South Pole and 0.8% of the time at Dome C (Figure 13g, Table S1). Near
714 surface stability stronger than SS occurs 12.3% to 33.4% of the time at the coastal sites and 68.8% to
715 96.9% of the time at the interior sites (Table S1), emphasizing the dominance of strong near surface
716 stability in the continental interior in winter. When considering the maximum stability below 500 m, it is
717 important to note that even though about half the time WS and weaker regimes occur near the surface at
718 the coastal sites, above the boundary layer enhanced stability remains. MS and stronger stability within
719 the lowest 500 m of the atmosphere occurs 72.1% to 91.6% of the time at the coastal sites. (Figure 13h,
720 Table S1). While there are very few cases with WS or weaker near surface stability at the continental
721 interior sites in the winter these always have enhanced stability above the boundary layer (Figure 13h).
722 The maximum stability below 500 m at the interior sites is almost always MS and stronger (99.8% to
723 100%), but in fact, the maximum stability is almost just as often SS or stronger (99.2% to 99.6%) (Table
724 S1). This emphasizes the near complete dominance of the SS, VSS, and ESS regimes in the continental
725 interior during the winter, while these regimes represent half or fewer (18.2% to 54.3%) of cases when
726 considering maximum stability below 500 m at the coastal sites in the winter (Figure 13h, Table S1).

727 It is also interesting to note the frequency of stability regimes in the spring and fall in comparison
728 to that in the summer and winter at all five sites. At the interior sites, there is a tendency for the regime
729 frequencies, whether considering just near surface stability or the maximum stability in the lowest 500 m,
730 in the fall and spring to mirror the winter season regime frequencies, and summer is completely distinct
731 from the other seasons (Figure 13c through 13j, Table S1). The most common near-surface stability
732 groupings in the fall and spring are WS and weaker at the coastal sites (55.7% to 71.8% of the time;
733 Figures 13e and 13i), and these regimes are observed less frequently in the transition seasons than they
734 are in the summer (80.1% to 92.1%; Figure 13c), but more frequently than in the winter (40% to 53.6%;
735 Figure 13g). In comparison, the transition seasons at the continental interior sites are usually characterized
736 by MS and stronger stability near the surface (77.7% to 95.4%; Figure 13f and 13j), which is similar to
737 the frequency of these regimes in the winter as well (85.8% to 99.5%; Figure 13g). Thus, at the interior
738 sites, this comparison emphasizes the quick descent into winter-like conditions in the transition seasons,
739 whereas at the coastal sites, this change is more gradual.



740 *Figure 13: Summary of the basic near-surface stability regime frequency (left column) and aloft stability regime frequency (right column) at all five sites annually (top row) and seasonally: summer, fall, winter*
 741 *and spring (bottom four rows). The colored bars indicate the frequency of each of the given regimes at each site: South Pole (dark blue), Dome C (light blue), McMurdo (yellow), Neumayer (orange), and*
 742 *Syowa (red).*
 743
 744



745 To assess how applicable the commonly cited clear, strongly stable and cloudy, weakly stable
746 description of polar winter boundary layers (Stone and Kahl, 1991; Mahrt et al., 1998; Mahrt, 2014;
747 Solomon et al., 2023) is for the Antarctic we applied the method of Solomon et al. (2023) to identify clear
748 and cloudy conditions, based on net longwave radiation. This approach for identifying clear and cloudy
749 conditions was successful at the coastal Antarctic sites (Figures S3 to S5) but was unable to identify
750 distinct radiative signatures for clear or cloudy conditions at the two interior sites (Figures S1 and S2).
751 This suggests there may be fundamental differences in processes related to clouds, radiation, and stability
752 on the polar plateau in comparison to the coastal region of Antarctica or over Arctic sea ice. Vignon et al.
753 (2017) suggested that there may be two distinct boundary layer regimes (weakly stable and strongly
754 stable) at Dome C, but contrary to locations in the Arctic (Solomon et al., 2017), this is likely due to a
755 critical shift in wind speeds, not a bimodal distribution in radiative forcing (Vignon et al., 2017).

756 For the three coastal sites, the frequency of the 20 boundary layer stability regimes defined in
757 Table 2 was calculated for clear and cloudy conditions (Figure 12). This analysis revealed MS and
758 stronger regimes occur more often with clear conditions rather than cloudy conditions at McMurdo and
759 Neumayer. The NN and WS regime grouping at McMurdo (excluding NN-SSA) and the NN regime
760 grouping at Neumayer occur more often with cloudy rather than clear conditions, but these are the only
761 stability regimes in this analysis in which there is a large difference in frequency for cloudy or clear
762 conditions. At Syowa, there is little difference in the frequency of any stability regime for both clear and
763 cloudy conditions. The fact that some stability regimes at McMurdo and Neumayer and all the stability
764 regimes at Syowa show little sensitivity to changes in cloud cover suggest a more nuanced relationship
765 between radiative forcing and near-surface stability may exist in the Antarctic compared to the Arctic, and
766 other forcing mechanisms, such as mechanical mixing, may be relatively more important in distinguishing
767 boundary-layer stability regimes from one another. Mahrt (2014) noted that weakly stable conditions
768 occur with either cloud cover or increased wind and mentioned that classification into the weakly stable
769 and strongly stable regimes does not encompass the full complexity of forcing in the stable boundary
770 layer.

771 A useful next step in this research will be to more thoroughly assess the forcing for the different
772 stability regimes. Largely, radiative forcing and mechanical mixing (wind shear) are two main drivers of
773 boundary layer stability. The role of these two processes, across seasons at the individual sites, but also
774 across the five sites will be the basis of continued research. Assessing forcing for regimes that showed
775 little sensitivity to cloud cover is of interest since it appears that changes in radiative forcing may not play
776 a dominant role. A paper following this study will use the boundary layer regimes identified for each
777 individual radiosonde profile to identify variations in radiation and wind speed associated with the
778 different stability regimes. Further, an analysis of the ability of the Antarctic Mesoscale Prediction
779 System (AMPS, Powers et al., 2012) to simulate the range of stability regimes observed at each site and
780 the radiative and mechanical forcing associated with these regimes across Antarctica is planned.



781 **Data Availability**

782 The data used to support this project can be found at:

783 McMurdo:

784 All data: https://adc.arm.gov/discovery/#/results/site_code::awr.

785 Syowa:

786 Radiosonde data: Office of Antarctic Observation Japan Meteorological Agency (pers. comm.
787 Yutaka Ogawa)

788 Radiation data: <https://doi.pangaea.de/10.1594/PANGAEA.956748>

789 Dome C:

790 Radiosonde data: <https://www.climantartide.it/dataaccess/rds/index.php?lang=it&rds=DOMEC>

791 Radiation data: <https://doi.pangaea.de/10.1594/PANGAEA.935421>

792 South Pole:

793 Radiosonde data: <http://amrc.ssec.wisc.edu/data/ftp/pub/southpole/radiosonde/>

794 Radiation data: <https://doi.pangaea.de/10.1594/PANGAEA.956847>

795 Neumayer:

796 Radiosonde data: <https://doi.org/10.1594/PANGAEA.940584>

797 Radiation data: <https://doi.org/10.1594/PANGAEA.940584>

798 **Competing Interests**

799 The contact author has declared that none of the authors has any competing interests.

800 **Acknowledgements**

801 Funding for this work came from the United States National Science Foundation (NSF) grant OPP
802 1745097 and the National Aeronautics and Space Administration (NASA; award 80NSSC19M0194). The
803 authors thank the United States Antarctic Program, the Department of Energy, the Baseline Surface
804 Radiation Network, the Antarctic Meteorological Research and Data Center, the Antarctic Meteo-
805 Climatological Observatory, and the Office of Antarctic Observation Japan Meteorological Agency for
806 the support and logistics for the data used in this paper.

807 **References**

808 Andreas, E.L., Claffy, K.J., and Makshtas, A.P.: Low-level atmospheric jets and inversions over the
809 western Weddell Sea, *Boundary-Layer Meteorology*, 97, 459-486, doi:10.1023/A:1002793831076, 2000.

810 Aristidi, E., Agabi, K., Azouit, M., Fossat, E., Vernin, J., Travouillon, T., Lawrence, J.S., Meyer, C.,
811 Storey, J.W.V., Halter, B., Roth, W.L., and Walden, V.: An analysis of temperatures and wind speeds
812 above Dome C, Antarctica, *Astronomy and Astrophysics*, 430, 739-746. doi:10.1051/0004-
813 6361:20041876, 2005.



- 814 Comiso, J. C.: Surface temperatures in the polar regions from Nimbus 7 temperature humidity infrared
815 radiometer, *Journal of Geophysical Research*, 99, 5181-5200. <https://doi.org/10.1029/93JC03450>, 1994.
- 816 Cassano, E.N., Glisan, J.M., Cassano, J.J., Gutowski, W.J. Jr., and Seefeldt, M.W.: Self-organizing map
817 analysis of widespread temperature extremes in Alaska and Canada, *Climate Research*, 62, 199-218,
818 <https://doi.org/10.3354/cr01274>, 2015.
- 819 Cassano, J. J., Nigro, M., and Lazzara, M.: Characteristics of the near surface atmosphere over the Ross
820 ice shelf, Antarctica, *Journal of Geophysical Research: Atmospheres*, 121, 3339-3362,
821 <https://doi.org/10.1002/2015JD024383>, 2016.
- 822 Dice, M. J., and Cassano, J. J.: Assessing physical relationships between atmospheric state, fluxes, and
823 boundary layer stability at McMurdo Station, Antarctica, *Journal of Geophysical Research: Atmospheres*,
824 127, e2021JD036075. <https://doi.org/10.1029/2021JD036075>, 2022.
- 825 Genthon, C., Six, D., Gallée, H., Grigioni, P., and Pellegrini, A.: Two years of atmospheric boundary
826 layer observations on a 45-m tower at Dome C on the Antarctic plateau, *Journal of Geophysical Research:*
827 *Atmospheres*, 118, 3218-3232, doi:10.1002/jgrd.50128, 2013.
- 828 Hewitson, B. C., and Crane, R. G.: Self-organizing maps: Applications to synoptic climatology, *Climate*
829 *Research*, 22, 13-26. <https://doi.org/10.3354/cr022013>, 2002.
- 830 Hudson, S., and Brandt, R.: A look at the surface-based temperature inversion on the Antarctic Plateau,
831 *Journal of Climate*, 18, 1673-1696, <https://doi.org/10.1175/JCLI3360.1>, 2005.
- 832 Jozef, G., Cassano, J., Dahlke, S., and de Boer, G.: Testing the efficacy of atmospheric boundary layer
833 height detection algorithms using uncrewed aircraft system data from MOSAiC, *Atmospheric*
834 *Measurement Techniques*, 15, 4001-4022, <https://doi.org/10.5194/amt-15-4001-2022>, 2022.
- 835 Jozef, G. C., Cassano, J. J., Dahlke, S., Dice, M., Cox, C. J., and de Boer, G.: An Overview of the
836 Vertical Structure of the Atmospheric Boundary Layer in the Central Arctic during MOSAiC, EGU sphere
837 [preprint], <https://doi.org/10.5194/egusphere-2023-780>, 2023.
- 838 King, J. C. and Turner, J.: *Antarctic Meteorology and Climatology*, Cambridge Atmospheric and Space
839 Sciences Series, Cambridge University Press, U.K., 1997.
- 840 Kohonen, T., Hynninen, J., Kangas, J., and Laaksonen, J.: SOMPAK: The Self-Organizing Map Program
841 Package, Rep. A31, Lab. Of Comput. and Inf. Sci., Helsinki Univ. of Technol., Espoo, Finland, 1996.
- 842 König-Langlo, G. and Loose, B.: The Meteorological Observatory at Neumayer Stations (GvN and NM-
843 II) Antarctica, *Polarforschung*, 76, 25-38, hdl:10013/epic.28566.d001, 2007.
- 844 Lettau, H. H., and Schwerdtfeger, W.: *Antarctic J. U.S.* 2, 155-158. 1967.
- 845 Lubin, D., Bromwich, D. H., Vogelmann, A. M., Verlinde, J., and Russell, L. M.: ARM West Antarctic
846 Radiation Experiment (AWARE) Field Campaign Report, DOE/SC-ARM-17-028, 2017.
- 847 Lubin, D., Zhang, D., Silber, I., Scott, R. C., Kalogeras, P., Battaglia, A., et al.: AWARE: The
848 atmospheric radiation measurement (ARM) West Antarctic radiation experiment. *Bulletin of the*
849 *American Meteorological Society*, 101, E1069-E1091, <https://doi.org/10.1175/BAMS-D-18-0278.1s>,
850 2020.



- 851 Mahesh, A., Walden, V. P., and Warren, S. G.: Radiosonde Temperature Measurements in Strong
852 Inversions: Correction for Thermal Lag Based on an Experiment at the South Pole, *Journal of*
853 *Atmospheric and Oceanic Technology*, 14, 45-53. [https://doi.org/10.1175/1520-](https://doi.org/10.1175/1520-0426(1997)014<0045:RTMISI>2.0.CO;2)
854 [0426\(1997\)014<0045:RTMISI>2.0.CO;2](https://doi.org/10.1175/1520-0426(1997)014<0045:RTMISI>2.0.CO;2), 1997.
- 855 Mahrt, L.: Stratified atmospheric boundary layers and breakdown of models, *Theoretical and*
856 *Computational Fluid Dynamics*, 11, 263-280, 1998.
- 857 Mahrt, L.: Stably Stratified Atmospheric Boundary Layers, *Annual review of fluid mechanics*, 46, 23-45,
858 doi:10.1146/annurev-fluid-010313-141354, 2014.
- 859 Matsuoka, K., Skoglund, A., and Roth, G.: Quantarctica [data set]. Norwegian Polar Institute.
860 <https://doi.org/10.21334/npolar.2018.8516e961>, 2018.
- 861 Murakoshi, N.: Meteorological observations at the Syowa base during the period from March 1957 to
862 February 1958, Japan Meteorological Agency, doi/10.15094/00006856, 1958.
- 863 Nigro, M. A., Cassano, J. J., Wille, J., Bromwich, D. H., and Lazzara, M. A.: A Self-Organizing-Map-
864 Based Evaluation of the Antarctic Mesoscale Prediction System Using Observations from a 30-m
865 Instrumented Tower on the Ross Ice Shelf, Antarctica, *Weather and Forecasting*, 32, 223-242,
866 <https://doi.org/10.1175/WAF-D-16-0084.1>, 2017.
- 867 Phillpot, H. R., and Zillman, J. W.: The surface temperature inversion over the Antarctic
868 continent, *Journal of Geophysical Research*, 75, 4161-4169, <https://doi.org/10.1029/JC075i021p04161>,
869 1970.
- 870 Pietroni, I., Argentini, S., Petenko, I., and Sozzi, R.: Measurements and Parametrizations of the
871 Atmospheric Boundary-Layer Height at Dome C, Antarctica. *Boundary Layer Meteorology*, 143, 189-
872 206, <https://doi.org/10.1007/s1046-011-9675-4a>, 2012.
- 873 Powers, J. G., Manning, K. W., Bromwich, D. H., Cassano, J. J., and Cayette, A. M.: A Decade of
874 Antarctic Science Support Through AMPS, *Bulletin of the American Meteorological Society*, 93, 1699-
875 1712, doi: <https://doi.org/10.1175/BAMS-D-11-00186.1>, 2012.
- 876 Reusch, D.B., Alley, R.B., Hewitson, B.C.: Relative performance of self-organizing maps and principal
877 component analysis in pattern extraction from synthetic climatological data, *Polar Geography*, 29, 188-
878 212, <https://doi.org/10.1080/789610199>, 2005
- 879 Schwartz, B. E., and Doswell, C. A., III.: North American Rawinsonde Observations: Problems,
880 Concerns, and a Call to Action, *Bulletin of the American Meteorological Society*, 72, 1885-1896,
881 [https://doi.org/10.1175/1520-0477\(1991\)072<1885:NAROPC>2.0.CO;2](https://doi.org/10.1175/1520-0477(1991)072<1885:NAROPC>2.0.CO;2), 1991.
- 882 Silber, I., Verlinde, J., Eloranta, E. W., and Cadetdu, M.: Antarctic Cloud macrophysical, thermodynamic
883 phase, and atmospheric inversion coupling properties at McMurdo station: I. Principal data processing
884 and climatology. Antarctic cloud macrophysical, thermodynamic phase, and atmospheric inversion
885 coupling properties at McMurdo Station: I, Principal data processing and climatology, United States, 123,
886 6099-6121, <https://doi.org/10.1029/2018JD028279>, 2018.
- 887 Silva, T., Schlosser, E., and Lehner, M.: A 25-year climatology of low-tropospheric temperature and
888 humidity inversions for contrasting synoptic regimes at Neumayer Station, Antarctica, *International*
889 *Journal of Climatology*, 43, 456-479, <https://doi.org/10.1002/joc.7780>, 2022



- 890 Solomon, A., Shupe, M.D., Svensson, G., Barton, N.P., Batrak, Y., Bazile, E., Day, J.J., Doyle, J.D.,
891 Frank, H.P., Keeley, S., Remes, T., Tolstykh, M.: The winter central Arctic surface energy budget: A
892 model evaluation using observations from the MOSAiC campaign. *Elementa: Science of the*
893 *Anthropocene*; 11, 00104, doi: <https://doi.org/10.1525/elementa.2022.00104>, 2023
- 894 Stone, R. S., and Kahl, J. D.: Variations in boundary layer properties associated with clouds and transient
895 weather disturbances at the South Pole during winter, *Journal of Geophysical Research*, 96, 5137-5144,
896 doi:10.1029/90JD02605, 1991.
- 897 Stull, R. B.: *An Introduction to Boundary Layer Meteorology*, Springer, 1988.
- 898 Vignon, E., van de Wiel, B. J. H., van Hooijdonk, I. G. S., Genthon, C., van der Linden, S. J. A., van
899 Hooft, J. A., Baas, P., Maurel, W., Traulle, O., and Casasanta, G.: Stable boundary-layer regimes at Dome
900 C, Antarctica: observation and analysis, *Quarterly Journal of the Royal Meteorological Society*, 143,
901 1241, <https://doi.org/10.1002/qj.2998>, 2017.
- 902 Yamada, K., and Hirasawa, N.: of a Record-Breaking Strong Wind Event at Syowa Station in January
903 2015, *Journal of Geophysical Research: Atmospheres*, 123, 13643-13657.
904 <https://doi.org/10.1029/2018JD028877>, 2018.
- 905 Zhang, Y., Seidel, D., Golaz, J., Deser, C., and Tomas, R.: Climatological characteristics of Arctic and
906 Antarctic surface-based inversions, *Journal of Climate*, 24, 5167-5186.
907 <https://doi.org/10.1175/2011JCLI4004.1>, 2011.